AN URBAN SURFACE EXCHANGE PARAMETERISATION FOR MESOSCALE MODELS

ALBERTO MARTILLI[1,⋆], ALAIN CLAPPIER[1] and MATHIAS W. ROTACH[2]
[1]*Swiss Federal Institute of Technology, Lausanne (EPFL), Air and Soil Pollution Laboratory, 1015-Lausanne, Switzerland;* [2]*Swiss Federal Institute of Technology, Zurich (ETHZ), Institute for Climate Research, 8057-Zurich, Switzerland*

(Received in final form 20 November 2001)

Abstract. A scheme to represent the impact of urban buildings on airflow in mesoscale atmospheric models is presented. In the scheme, the buildings are not explicitly resolved, but their effects on the grid-averaged variables are parameterised. An urban quarter is characterised by a horizontal building size, a street canyon width and a building density as a function of height. The module computes the impact of the horizontal (roof and canyon floor) and vertical (walls) surfaces on the wind speed, temperature and turbulent kinetic energy. The computation of the shortwave and longwave radiation, needed to compute the temperature of the urban surfaces, takes into account the shadowing and radiation trapping effects induced by the urban canyons. The computation of the turbulent length scales in the TKE equation is also modified to take into account the presence of the buildings.

The parameterisation is introduced into a mesoscale model and tested in a bidimensional case of a city over flat terrain. The new parameterisation is shown to be able to reproduce the most important features observed in urban areas better than the traditional approach which is based only on the modification of the roughness length, thereby retaining the Monin–Obukhov similarity theory. The new surface exchange parameterisation is furthermore shown to have a strong impact on the dispersion characteristics of air pollutants in urban areas.

Keywords: Air pollution, Mesoscale models, Street canyon, Urban boundary layer, Urban climatology, Urban energy balance.

1. Introduction

The main reason for the complexity of urban air quality problems lies in the diversity of spatio-temporal scales over which the phenomena occur. In particular, two important scales are involved:

1. An 'urban' scale of a few tens of kilometres (i.e., a normal city size) where large amounts of primary pollutants are emitted,
2. A 'meso' scale of a few hundreds of kilometres where the secondary pollutants are formed and dispersed.

Therefore, pollutant dispersion is strongly dependent on the structure of the urban boundary layer and on its interactions with the rural boundary layer and the synoptic flow.

⋆ Corresponding address: University of British Columbia, Department of Earth and Ocean Sciences, 6339 Stores Road, Vancouver, B.C., Canada V6T 1Z4. E-mail: amartilli@eos.ubc.ca

Boundary-Layer Meteorology **104:** 261–304, 2002.

Since this system is highly non-linear it is common to use numerical models to study air pollution problems. In order to compute the mean and turbulent transport and the chemical transformations of pollutants, several meteorological variables are needed (wind, turbulent coefficients, temperature, pressure, humidity), which can be interpolated from measurements or computed with mesoscale circulation models. These models must, indeed, ideally be able to represent the two main scales (the 'urban' and the 'meso') involved. Since the horizontal dimensions of the domain are on the order of the mesoscale (100 km), to keep the number of grid points compatible with the CPU time cost, the horizontal grid resolution of such (mesoscale) models ranges, in general, between several hundreds of metres and a few kilometres. This means that it is not possible to resolve the city structure in detail (buildings or blocks), but that the effects of the urban surfaces must be parameterised. Another obstacle to a complete resolution of the city structure is given by the difficulty to provide the necessary input data.

The most important urban effects on the airflow are (e.g., Roth, 2000):

- The presence of an intense shear layer at the top of the canopy. There, the mean kinetic energy of the flow is converted into turbulent kinetic energy.
- The development of wake diffusion. The turbulent wakes, generated by roughness elements, efficiently mix and diffuse momentum, heat, moisture and other scalars such as pollutants. The size of these eddies is related to the dimensions of the roughness elements.
- Drag due to buildings, i.e. the pressure differences across individual roughness elements.
- Differential heating/cooling of sunlit/shaded surfaces, radiation trapping effects in street canyons and heat storage in buildings. These phenomena can generate the so- called urban heat island effect.

The traditional technique used to represent the effects of the surface in mesoscale models is based on the constant-flux layer approximation in the surface layer (Monin-Obukhov similarity theory, or MOST). However, a series of field measurements (e.g., Rotach, 1993) has shown that this approach is not able to reproduce the vertical structure of the turbulent fields in the so-called urban roughness sublayer (RSL from street level up to heights of 50–100 m). In this paper, the impact of an improvement in the RSL representation on the flow and dispersion characteristics at mesoscale is analysed. In fact, if the mesoscale model is used to provide meteorological fields for pollutant dispersion models, the precision in this region, where pollutants are emitted and people live, is very important. Furthermore, in standard mesoscale models, the surface temperature is computed from the surface energy balance, which does not take into account shadowing and radiation trapping effects.

In the last few years, several efforts have been made in order to improve the representation of urban surface characteristics in mesoscale models. A good review of these methods can be found in Brown (2000). In general, attempts have been

made either to improve the 'dynamical' part (impact on the wind field and the turbulent kinetic energy) or the 'thermal' part (impact on the sensible heat fluxes).

For the former, many models maintain a MOST approach, with some improvements or modifications (see for example, Bottema, 1997). In these models, the lowest model level is close to the canopy height (the displacement height) rather than at the top of the RSL, and the values of roughness length and displacement height parameters are evaluated from roughness classifications or morphometric models (Grimmond and Oke, 2000). The drag-force (e.g., Uno et al, 1989) can be an alternative approach. In this formulation, a term is added in the momentum and turbulent kinetic energy (TKE) equations to account for obstacle drag, as is often done for vegetation canopies. With this technique, the lowest model level is at ground (or street) level.

With respect to the thermal properties of an urban surface, the surface energy balance is often modified. An interesting approach to take into account shadowing and radiative trapping effects by roughness elements is that of Masson (2000).

The approach presented here combines the drag approach for momentum and TKE with a method very similar to that presented by Masson (2000) for the sensible heat exchange. The method consists of taking into account the impact of horizontal (canyon floor, roof) and vertical (walls) surfaces in the momentum, heat and turbulent kinetic energy equations. This parameterisation is implemented in a mesoscale model and tested in a simple two-dimensional (2D) case.

Section 2 gives an overview of the mesoscale model used in this study. In Section 3, the methodology used to represent the city is presented and, in Sections 4 and 5, the technique adopted to compute the fluxes from the urban surfaces is described. In Section 6 the modifications introduced in the computation of the turbulent length scales are presented. The results of the simulations are described and analysed in Section 7 and the impact of the new parameterisation on the CPU time is discussed in Section 8. Finally, conclusions and perspectives are given in Section 9. The technique used to compute the radiation reflection in the urban canyon is described in details in Appendix A, and the average/interpolation procedures adopted to connect the urban and the mesoscale grid are given in Appendix B.

2. The Mesoscale Model

A mesoscale model (Clappier et al., 1996) has been developed, and solves the following conservation equations:

- Mass

$$\frac{\partial \rho U_i}{\partial x_i} = 0, \tag{1}$$

where U_i are the three wind components and ρ is the air density. In this equation the time variation of the density has been neglected (anelastic approximation). Here,

and in the following, capital letters denote Reynolds averaged variables, while small letters stand for their respective turbulent fluctuations.

- Momentum

$$\frac{\partial \rho U_i}{\partial t} = -\frac{\partial P}{\partial x_i} + F_i \tag{2}$$

with

$$F_i = -\frac{\partial \rho U_i U_j}{\partial x_j} - \frac{\partial \rho \overline{u_i w}}{\partial z} - \rho \frac{\theta'}{\theta_0} g \delta_{i3} - 2\varepsilon_{ijk}\Omega_j (U_k - U_k^G) + D_{u_i}.$$

Here, the first term on the right-hand side represents the mean transport and the second the turbulent transport (for which only the vertical direction is taken into account); P is the pressure, θ_0 is the potential temperature of the reference hydrostatic state and $\theta' = \theta - \theta_0$ is the fluctuation relative to this state, g is the gravity acceleration, Ω_j is the rotation angular velocity of the earth and U_k^G is the geostrophic wind. D_{u_i} here represents the forces (e.g., frictional force, drag force etc.) induced by the interactions between the 'solid' surfaces (ground, building etc.) and the airflow. Equation (2) is in the non-hydrostatic form and the buoyancy term is written using the Boussinesq approximation.

- Energy

$$\frac{\partial \rho \theta}{\partial t} = -\frac{\partial \rho \theta U_i}{\partial x_i} - \frac{\partial \rho \overline{w\theta}}{\partial z} + D_\theta - \frac{1}{C_p}\left(\frac{P_0}{P}\right)^{R/C_p} \frac{\partial R_{\text{lwave}}}{\partial z} \tag{3}$$

where θ is the potential temperature, C_p is the specific heat at constant pressure of the air, R is the gas constant, P_0 is the reference pressure (1000 hPa) and R_{lwave} is the longwave radiation flux. D_θ denotes the impact of the sensible heat fluxes from the 'solid' surfaces (ground or buildings) on the potential temperature budget.

- Air Humidity

$$\frac{\partial \rho H}{\partial t} = -\frac{\partial \rho H U_i}{\partial x_i} - \frac{\partial \rho \overline{wh}}{\partial x_i} + D_h \tag{4}$$

with H the mean absolute humidity of the air and h the turbulent fluctuation; here, no condensation and cloud formations are considered. D_h represents the impact of the latent heat fluxes from ground on the humidity budget.

In the numerical resolution, the mass Equation (1) is combined with the momentum Equation (2) to yield the following Poisson equation:

$$\frac{\partial}{\partial x_i}\left(\frac{\partial P}{\partial x_i}\right) = \frac{\partial F_i}{\partial x_i}. \tag{5}$$

Equations (2–5) are solved explicitly except for the pressure, which is solved implicitly. Following the technique of Rhie and Chow (1983) the terms F_i are estimated using wind speed and potential temperature at time n. Then, with these values of F_i, the pressure at time $n+1$ is computed from Equation (5). This pressure field is used to compute the new velocities from Equation (2).

The spatial discretisation is based on the finite volume method. The pressure gradients and the velocity fluxes are estimated at the faces of a cell, while the velocity components, the potential temperature, the air humidity and the pressure are located at the centre of the cells. The meshes are structured (each cell has six faces and it is connected with six neighbours). For the application presented in this paper the meshes are Cartesian, since the terrain is flat, but it is possible to represent a terrain-following grid in the case of complex terrain, by modifying the position of the cell's corner (deformable mesh). The mean transport is computed with a third-order parabolic piecewise method (PPM, Collella and Woodward, 1984) corrected for multidimensional applications (Clappier, 1998).

Above the ground surface, the vertical fluxes due to the turbulent transport are computed using the K-theory approach, viz.

$$\overline{wa} = -K_z \frac{\partial A}{\partial z}, \tag{6}$$

where A is the mean part (and a the turbulent part) of a variable that may be the potential temperature, the air humidity or one of the three components of the wind, and K_z is the diffusion coefficient. In order to compute the coefficient K_z, a $k-l$ closure based on Bougeault and Lacarrere (1989) is used (note that in the formulation of Bougeault and Lacarrere, the turbulent coefficients for momentum and for heat are equal). A prognostic equation for the turbulent kinetic energy, E, is used,

$$\frac{\partial \rho E}{\partial t} = -\frac{\partial \rho U_i E}{\partial x_i} - \frac{\partial \rho \overline{ew}}{\partial z} + \underbrace{\rho K_z \left[\left(\frac{\partial U_x}{\partial z} \right)^2 + \left(\frac{\partial U_y}{\partial z} \right)^2 \right] - \frac{g}{\theta_0} \rho K_z \frac{\partial \theta}{\partial z}}_{\text{Pr}}$$

$$- \underbrace{\rho C_\varepsilon \frac{E^{3/2}}{l_\varepsilon}}_{\text{dissip.}} + D_E \tag{7}$$

where Pr is the sum of the shear and buoyant production terms of turbulent kinetic energy. D_E again stands for the source of TKE generated by the interactions between the buildings and the airflow. The vertical diffusion coefficients are computed according to,

$$K_z = C_k l_k E^{1/2}. \tag{8}$$

In (7) and (8) C_k and C_ε are model parameters set equal to 0.4 and 0.71 respectively.

The two length scales in (7) and (8), l_k and l_ε, are determined by solving the following set of equations:

$$\int_z^{z+l_{\text{up}}} \beta(\theta(z) - \theta(z'))\mathrm{d}z' = E(z) \tag{9a}$$

$$\int_{z-l_{\text{down}}}^{z} \beta(\theta(z') - \theta(z))\mathrm{d}z' = E(z) \tag{9b}$$

$$l_\varepsilon = (l_{\text{up}} l_{\text{down}})^{1/2} \tag{9c}$$

$$l_k = \min(l_{\text{up}}, l_{\text{down}}). \tag{9d}$$

Here, l_{up} and l_{down} are the distances that a parcel originating from level z, and having the TKE of level z ($E(z)$), can travel upward and downward before coming to rest due to buoyancy effects (the Bougeault and Lacarrere (1989) formulation assumes the presence of a stable layer at a certain height above ground, in general the boundary-layer height); l_{down} cannot be greater than the height above the ground ($l_{\text{ground}} = z$).

At the ground turbulent fluxes of momentum, heat and water vapour are computed using the MOST according to the formulation of Louis (1979) in the standard mesoscale model. This parameterisation requires for every grid cell a value for the roughness length, surface temperature and moisture. The roughness length can be derived from land use data, while the temperature and moisture of the surface are computed by means of a soil module (Tremback and Kessler, 1985). This module solves two prognostic equations for temperature and water content at several levels in the soil. The boundary conditions at the deepest level in the soil (usually at about 1m below the surface) are kept constant in time, while at the interface between soil and atmosphere an energy budget, which takes into account solar radiation, incoming and outcoming longwave radiation, latent and sensible heat fluxes, is used to define the boundary conditions for temperature and for the soil moisture equation.

The solar radiation at the surface is computed using the formulation of Schayes (1982), including a specified aerosol absorption factor, variable earth-sun distance, dry air Rayleigh scattering and water vapour absorption. The downward longwave radiation flux is computed with the Sasamori (1968) scheme, which takes into account water vapour and carbon dioxide concentrations in the atmosphere. The same formulation is used for the evaluation of the infrared flux divergence term in Equation (3).

The dynamical part of the model has been validated using the analytical solution for mountains waves and for the well-known Boulder Storm (Clappier et al., 1997). Moreover the model has been applied to the MESOCOM experiment of

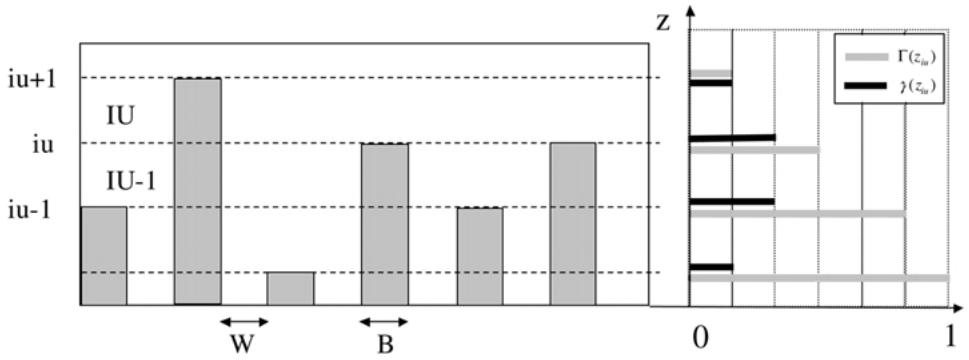

Figure 1. Schematic representation of the numerical grid in the urban module. W is the width of the street, B is the width of the buildings, iu are the face and IU the centre of the urban model levels. $\gamma(z_{iu})$ is the density of building of height z_{iu} and $\Gamma(z_{iu})$ is the density of building higher than z_{iu}.

intercomparison of mesoscale models (http://rtmod.ei.jrc.it/mesocom/) and it has been used over Athens, Greece (Martilli, 2001).

In the following sections the methodology used to describe the surface fluxes in the case of an urban-type surface is presented. In other words, the scheme to determine the D terms in Equations (2–4) and (7) is outlined in detail.

3. Urban Model

A city is probably one of the most complex existing surfaces. A complete reproduction of all the heterogeneity of a 'real' city would be too complex and hardly realisable in most cases due to the lack of detailed data. A simplification is therefore needed. However, the traditional approach usually adopted in mesoscale models (consisting in modifying the roughness length at the surface and the thermal properties of the ground) fails to reproduce the vertical structure of the turbulent momentum fluxes and the urban heat island effects. The main reason for this failure is that in this traditional approach the only sink of momentum is at the ground and is not distributed up to the higher buildings, and that the shadowing and radiation trapping effects are neglected. The new formulation must take into account these two effects.

We propose to represent the city as a combination of several urban classes. Every class is characterised by an array of buildings of the same width B located at the same distance from each other (canyon width W), but with different heights h (with a certain probability $\gamma(h)$ to have a building with height h, see Figure 1). To simplify the formulation we assume that the length of the street canyons is equal to the horizontal grid size. Starting from these data it is possible to compute the areas of every urban surface type (canyon floor, roof and walls) for each grid cell.

In order to give to the users the greatest flexibility in choosing the parameters, the urban structure is defined on a numerical grid different from the grid of the

mesoscale model. In the following (considering only the vertical direction), all the variables with index IU refer to the *Urban grid*, while variables with index I refer to the grid of the mesoscale model. Moreover, we adopt the convention in denoting the horizontal face of the numerical cells with lower case indices and the centre of the numerical cells with capital indices, or $iu = IU - 1/2$ for the urban grid and $i = I - 1/2$ for the grid of the mesoscale model.

3.1. Estimation of the areas of the urban surface types

Referring to a vertical numerical grid characterised by levels z_{iu},* the total area of horizontal surfaces at level iu, S^H_{iu}, is given by

$$S^H_{iu=1} = \frac{W}{W+B} S^H_{\text{tot}}, \tag{10a}$$

$$S^H_{iu>1} = \frac{B}{W+B} \gamma(z_{iu}) S^H_{\text{tot}}, \tag{10b}$$

where S^H_{tot} is the total horizontal area of the cell. Similarly, vertical surfaces are:

$$S^V_{IU} = \frac{\Delta z_{IU}}{W+B} \Gamma(z_{iu+1}) S^H_{\text{tot}}, \tag{11}$$

with Δz_{IU} vertical grid spacing and $\Gamma(z_{iu+1})$ is the probability to have a building with a height equal or greater than z_{iu+1} (Figure 1), or

$$\Gamma(z_{iu}) = \sum_{ju=iu}^{nu} \gamma(z_{ju}). \tag{12}$$

Here, nu is the highest level in the urban grid. Several directions can be defined for every urban class, and the model computes the impact of the urban surfaces for every direction defined in the class and then averages the results.

4. Computation of the Effects of the Urban Surfaces on the Airflow

As explained above, the most important effects of the urban surfaces on the airflow are: (i) drag induced by buildings with consequent loss of momentum, (ii) enhancement of the transformation of mean kinetic energy into turbulent kinetic energy, and (iii) modification of the heat fluxes due to shadowing and radiation trapping effects. The present method consists in computing the impact of every urban surface type (canyon floor, roofs and walls) on the momentum, heat and turbulent kinetic energy equation separately. These (additional) terms are then taken into account in proportion to the area of their respective surface fractions.

* z_{iu} is the height of the face of the iu-th level above the canyon floor. See Figure 1.

4.1. MOMENTUM

The presence of horizontal surfaces such as roofs or canyon floors induces a frictional force with consequent loss of momentum. This term is similar to that usually present in mesoscale models to represent the impact of the ground surface. The difference is that this term is distributed along the vertical, from ground up to the highest building, and it is proportional to the fractional area of the horizontal surfaces present in the cell.

Even if the applicability of MOST in this case is questionable, in the absence of an alternative theory, the classical surface-layer formulae (as in Louis, 1979) are used to compute the momentum flux for horizontal surfaces at every level. The turbulent momentum flux due to the horizontal surfaces (roofs and canyon floors) at the level iu is then*

$$\vec{F}u_{iu}^{H} = -\rho \frac{k^2}{\left[\ln\left(\frac{\Delta z_{IU}/2}{z_{0iu}}\right)\right]^2} f_m\left(\frac{\Delta z_{IU}/2}{z_{0iu}}, Ri_B\right) |U_{IU}^{\mathrm{hor}}| \vec{U}_{IU} S_{iu}^{H}, \tag{13}$$

where U_{IU}^{hor} is the horizontal component of the wind, Ri_B is the bulk Richardson number at the level IU (computed with the wind and temperature of that level) and f_m are the expressions used in Louis (1979), k is the von Karman constant equal to 0.4. This means that the flux at level iu is computed using the wind speed and air temperature at level IU, the temperature and the roughness length of the horizontal surfaces (canyon floor or roofs) at level iu. It is important to note, here, that MOST is used to compute only the contribution of the horizontal surfaces (canyon floor and roofs). The roughness lengths are representative of the roughness of the specific surface types (roof or canyon floors) and not for the ensemble of the city.

The presence of the buildings induces pressure and viscous drag forces on the flow. The exchange of momentum on the vertical surfaces (walls) due to these forces is parameterised in the following way (see Raupach et al. (1991), for a rigorous justification of this approach):

$$\vec{F}u_{IU}^{V} = -\rho C_{\mathrm{drag}} |U_{IU}^{\mathrm{ort}}| \vec{U}_{IU}^{\mathrm{ort}} S_{IU}^{V}, \tag{14}$$

where $\vec{U}_{IU}^{\mathrm{ort}}$ is the wind speed orthogonal to the street direction at level IU and S_{IU}^{V} is the total surface of the walls at level IU. The value of the constant C_{drag} is set to 0.4 according to the measurements of Raupach (1992) in a wind tunnel with cubic arrays. This approach is very common in modelling the impact of obstacles (for example, it is used for vegetative canopy flows, see Wilson and Shaw (1977) or Yamada (1982), or Ayotte et al. (1999) and many others). For a city, this approach

* In order to avoid confusion, we denote the fluxes between the solid surfaces and the atmosphere with the symbol F and the turbulent fluxes in the atmosphere, arising from the Reynolds averaging process, with the symbol $\overline{wa}$ (see Equation (6)).

was used by Sievers (1990), Uno et al. (1989), Brown and Williams (1998) and Ashie et al. (1999). It is important to note here that in this formulation, the force induced by the presence of the buildings is orthogonal to the direction of the street canyon and it has a component against the horizontal wind direction. Dimensionally, the two components of this force can also be seen as the momentum flux components induced by the presence of the vertical surfaces of the buildings.

4.2. TEMPERATURE

In analogy with the momentum approach, the turbulent fluxes of sensible heat from roofs and the canyon floor (horizontal surfaces of the buildings) are computed according to:

$$F\theta_{iu}^{H} = -\rho \frac{k^2}{\left[\ln\left(\frac{\Delta z_{IU}/2}{z_{0iu}}\right)\right]^2} |U_{IU}^{\text{hor}}| \Delta\theta f_h \left(\frac{\Delta z_{IU}/2}{z_{0iu}}, Ri_B\right) S_{iu}^{H}. \tag{15}$$

Here $\Delta\theta$ is the difference between the air temperature and the surface temperature of the roof or canyon floor. As is described in the previous section, f_h refers to the expressions used in Louis (1979).

Temperature fluxes from the walls are also a function of the difference between the air temperature and the wall temperatures, but since walls are vertical surfaces Equation (15) cannot be used. Arnfield and Grimmond (1998) in their urban energy budget model propose a formulation by Clarke (1985) to compute the exchange of sensible heat coefficient as a function of the between-building wind speed. We adopt the same formulation here. For the case of a north-south street direction we have

$$F\theta_{IU}^{V} = -\frac{\eta}{C_p}\left[(\theta_{\text{air}} - \theta_{IU}^{\text{West}^{\text{wall}}}) + (\theta_{\text{air}} - \theta_{IU}^{\text{East}^{\text{wall}}})\right] S_{IU}^{V}. \tag{16}$$

Here $\theta_{IU}^{\text{West}^{\text{wall}}}$ and $\theta_{IU}^{\text{East}^{\text{wall}}}$ are the surface potential temperatures of the IU-th level of the West and East walls, respectively, and

$$\eta = c_c\left(a_c + b_c\left(\frac{U_{IU}^{\text{hor}}}{d_c}\right)\right), \tag{17}$$

where a_c, b_c, c_c, d_c are empirical constants equal to 1.09, 0.23, 5.678 and 0.3048, respectively.

In order to compute the surface temperatures of roofs, walls and streets a heat diffusion equation is solved at several levels in the material (concrete or asphalt), and an energy budget is computed for every surface. Details of these calculations are given in Appendix A.

4.3. TURBULENT KINETIC ENERGY

In many state-of-the-art mesoscale models, a turbulence closure involving a prognostic equation for the turbulent kinetic energy is used. In the classical approach, at the lowest model level the impact of the surface is taken into account in the shear and buoyant production terms of the turbulent kinetic energy (Pr in the Equation (7)) using the values of the surfaces fluxes and the MOST relationships. We adopt the same approach for the horizontal surfaces. These terms are multiplied, here, by a reference volume above that surface, since they are 'volumetric' (not fluxes),

$$\mathrm{Pr}_{iu}^{H} = \left[-\frac{(Fu_{iu}^{H}/\rho S_{iu}^{H})^{3/2}}{k \cdot \dfrac{\Delta z_{IU}}{2}} + \frac{g}{\theta_0} \frac{F\theta_{iu}^{H}}{\rho S_{iu}^{H}} \right] S_{iu}^{H} \Delta z_{IU} \rho, \tag{18}$$

where Δz_{IU} is the vertical size of the cell at level IU. It must be noted, here, that this is only a part of the total shear and buoyancy terms, i.e., that part induced by the horizontal surfaces (see Appendix B).

With considerations similar to those for momentum it is possible to show that the presence of the buildings increases the conversion of mean kinetic energy into turbulent kinetic energy (see, for example, Raupach and Shaw (1982) for a rigorous justification). In analogy with what it is done in many vegetation canopy models, the extra source term for TKE has the dimensions of a flux and it is parameterised as

$$Fe_{IU}^{V} = C_{\mathrm{drag}} |U_{IU}^{\mathrm{ort}}|^3 S_{IU}^{V}. \tag{19}$$

5. Computation of the 'Urban' Terms

The extra terms D_A in Equations (2), (3) or (7) (for a variable A that can be wind speed, temperature or TKE) in urban areas are equal to the fluxes due to the presence of buildings plus the fluxes due to the turbulent transport computed in the traditional way. In other words

$$D_{A_I} = \frac{Fa_I^H + Fa_I^V}{V_I^A}, \tag{20}$$

with V_I^A volume of air in the grid cell I and Fa_I^V, Fa_I^H are the average (interpolation to the grid of the mesoscale model) of the fluxes computed on the urban grid due to the presence of the buildings (see Figure 2).

The method used to numerically compute the turbulent transport in the vertical is also modified as follows:

$$\frac{\partial \rho \overline{wa}}{\partial z} = \frac{1}{V_I^A} (\rho \overline{wa}_i S_i^A - \rho \overline{wa}_{i+1} S_{i+1}^A), \tag{21}$$

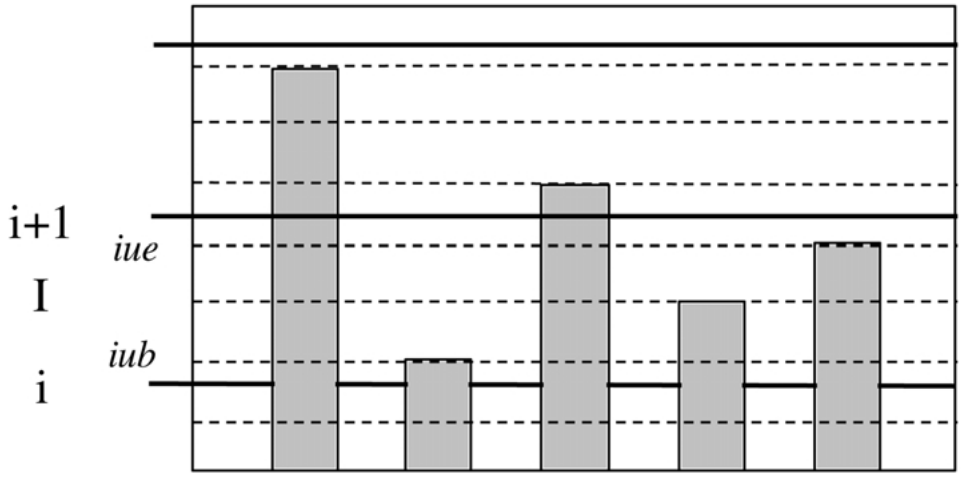

Figure 2. Representation of the connection between the urban module grid (dashed levels) and the mesoscale model grid (solid levels). iub and iue are the lowest and the highest urban model levels in the mesoscale level I.

where S_i^A is the surface between the grid cells I and grid cell $I-1$ not occupied by buildings. The methodology used to connect the two grids (averaging/interpolation procedures, computation of surfaces and volumes, etc.) is explained in detail in Appendix B.

6. Modification of the Turbulent Length Scales

There are several ways to compute the dissipation term in the TKE equation (Equation (7)). One possibility is to compute a complete prognostic equation for the dissipation ($k-\epsilon$ models, for example Duynkerke, 1988). Another possibility is to estimate the dissipation using the value of the turbulent kinetic energy and a dissipation length scale ($k-l$ models) as in the formulation of the dissipation term in Equation (7). The turbulent diffusion coefficients are then estimated using a mixing length and the turbulent kinetic energy (Equation (8)).

In the present model a $k-l$ formulation based on the work of Bougeault and Lacarrere (1989) is used. We therefore propose two 'urban' modifications of the length scales. Even if in this paper they are applied and tested only for the Bougeault and Lacarrere scheme, the modifications can easily be generalised and applied to any other 'standard' $k-l$ closure formulation.

The first modification is necessary because the presence of a building generates vortices of the building's spatial dimension. As a representative scale dimension of the building, we choose its height.⋆ Since there can be buildings of different height

⋆ The choice of height, instead of the width of the street or the minimum of the two, is mainly based on the assumption that the vortexes generated by the buildings have the same scale as the

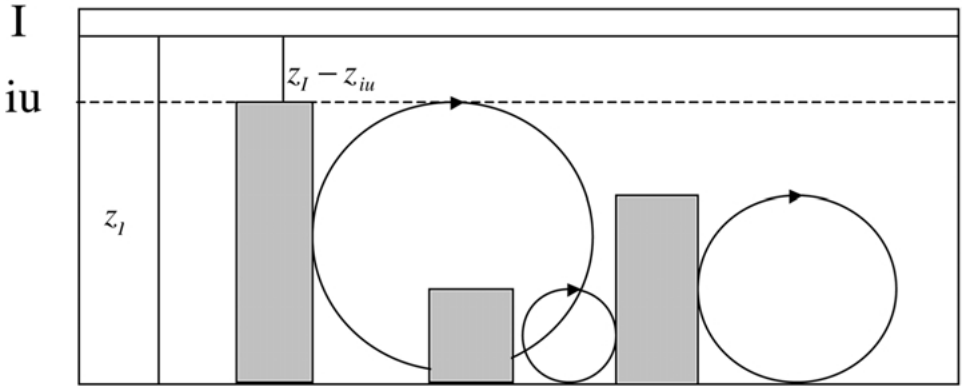

Figure 3. Schematic to illustrate the modification of the turbulent length scales.

in the grid cell, we assume that lower levels 'feel' the influence of higher and smaller buildings, while at higher levels only vortices induced by higher buildings are important (see Figure 3). The length scale, l_b, reflecting this process at level I is then

$$\left.\frac{1}{l_b}\right|_I = \sum_{iu=ibu}^{nu} \gamma(z_{iu}) \frac{1}{z_{iu}}. \tag{22}$$

Here, ibu is the lowest level of the urban grid where $z_I < z_{ibu}$ (z_I is the height of the centre of the mesoscale grid cell I). This new length scale is then added to the length scale computed with the traditional Bougeault and Lacarrere formulation, l_{old}:

$$\frac{1}{l} = \frac{1}{l_{\text{old}}} + \frac{1}{l_b}. \tag{23}$$

The modification is applied to both length scales, l_k and l_ε. It is obvious from Equation (22) that, for the model levels higher than the highest building, this correction is not active. This is equivalent to adding to the 'normal' dissipation ($\rho C_\varepsilon E^{3/2}/l_{\text{old}}$), a second dissipation ($\rho C_\varepsilon E^{3/2}/l_b$) linked with the scale of turbulence induced by the presence of the buildings. As a consequence, the net result of the presence of the buildings is to increase the cascade of energy from mean kinetic energy to TKE, and also to increase the dissipation rate.

building. Certainly, the width of the street can play a role, but, as a first approximation, we decided to neglect it in order to keep the parameterisation simple. At our knowledge, from the urban measurements of TKE already existing it is not possible to judge which choice is more appropriate. Further investigations with more accurate experimental data are needed to clarify this point. However, it must be noticed that in the simulation set-up used for this study, at all the levels in the urban canopy, the building height is similar or smaller than the street width (considered as the mean distance between two buildings).

The second modification is more strictly linked with the technique used to compute the traditional length scale. In the Bougeault and Lacarrere method, as in most of the more common $k-l$ closure techniques, an important parameter in the computation is the height above ground. In our case, in order to take into account the presence of buildings of different height, for level I the following value is used instead of the simple height above ground z_I:

$$l_{\text{ground}}|_I = \frac{1}{\left(\frac{W}{B+W}\right)\frac{1}{z_I} + \left(\frac{B}{B+W}\right)\sum_{iu=1}^{ibu-1}\gamma(z_{iu})\frac{1}{(z_I - z_{iu})}}. \tag{24}$$

This formula is a weighted average of the height above the canyon floor and the height above the roofs of the buildings.

7. Numerical Tests

The new urban parameterisation was implemented in the mesoscale model and tested in a simple 2D case.

7.1. Set-up of the simulations

The horizontal extension of the domain is 100 km with a resolution of 1 km. The vertical resolution is 10 m in the first 50 m above the ground (it is important, for the urban module, to have several levels in the urban canopy layer) and then it is stretched up to 1000 m at the top (6000 m). The topography is flat with a 10-km wide city (10 'urban' points) surrounded by a rural area.

In the city the width of the street canyons is assumed to be 20 m and the horizontal building size is fixed at 20 m. The probabilities of building heights are 20% for 10 m, 55% for 20 m, 20% for 30 m and 5% for 50 m. This situation is quite typical for downtown districts of a European city, corresponding to a majority of six storey buildings (around 20 m height), some smaller, some higher and some few very tall ones. The street canyons are oriented north-south (perpendicular to the 2D plane of the simulation). In Table I the values of other parameters are presented (albedo, roughness and thermal properties of the walls, the canyon floor and the roofs), and Table II lists the soil characteristics of the rural area.

The meteorological initial conditions are a geostrophic wind from the west of 2 m s^{-1} (used also as synoptic wind in the computation of the Coriolis force), an atmospheric thermal stratification equal to 3.5 K km^{-1} in potential temperature and a relative humidity of the air equal to 50% in the first 1000 m, and then reducing with height. A second simulation, with the same set- up, but with stronger geostrophic wind (5 m s^{-1}) was also performed to analyse the model behaviour in the case where mechanical effects are dominant.

TABLE I

Parameters for the city in *Urban* and *Trad* simulations. Here K_s is the substrate thermal conductivity of the material, C_s is the specific heat of the material, $T_{(\mathrm{int})}$ is the initial temperature of the material and also temperature of the deepest layer, ε is the emissivity of the surface, α is the albedo of the surface and z_0 is the roughness length of the surface.

Surface	K_s ($\mathrm{m^2\ s^{-1}}$)	C_s ($\mathrm{J\ m^{-3}\ K^{-1}}$)	$T_{(\mathrm{int})}$ (°C)	ε	α	z_0 (m)
Wall (*Urban*)	0.67×10^{-6}	1×10^{-6}	20	0.90	0.2	
Roof (*Urban*)	0.67×10^{-6}	1×10^{-6}	20	0.90	0.2	0.01
Floor (*Urban*)	0.29×10^{-6}	1.4×10^{-6}	17	0.95	0.2	0.01
Ground (*Trad*)	0.29×10^{-6}	1.4×10^{-6}	20	0.95	0.2	2.0

TABLE II

Rural parameters. Here α is the albedo, ε is the emissivity, z_0 is the roughness length and $T_{(\mathrm{int})}$ is the initial temperature and also the temperature of deepest level. The other characteristics of the soil type are those of the USDA (United States Department of Agriculture) Textural classes (see also Tremback and Kessler, 1985).

Soil type	α	ε	z_0 (m)	$T_{(\mathrm{int})}$ (°C)	Initial soil moisture
Sandy clay loam	0.2	0.95	0.1	17	0.5 of saturation

The boundary conditions are computed on a vertical column (the same equations of the model are solved, but neglecting the horizontal derivatives). The day of the simulation is 10 September and the latitude is 49° N; the simulation starts in the morning (0600 LST, around sunrise) and lasts for 3 days.

In order to evaluate the impact of the present parameterisations, another simulation with the same set-up, but with the city characterised only by a change in roughness length and the soil characteristics of concrete (see Table I), was performed. Several methods have been presented in the literature in order to determine the roughness length for an urban surface (see for example the review of Grimmond and Oke, 2000). For our control simulation, we have chosen the simplest method (called rule-of-the-thumb in Grimmond and Oke's paper) fixing the roughness length at 0.1 of the average building height (in the specific case the average building height is 20 m and accordingly the roughness length is 2 m). We note also that the building density chosen ($\lambda_p = 0.5$ in the notation of Grimmond and Oke's paper) is in the range of real cities and that all the methods presented in their paper gave a similar roughness length for this situation.

In the following description we will refer to the simulations made with the urban-specific formulation, as proposed in the present paper as '*Urban*' (urban

parameterisation), while the simulation performed with the classical MOST approach is denoted '*Trad*' (traditional approach).

7.2. RESULTS

In this section, a comparison between model results (for the simple case described above) and the available measurements in the literature is made for momentum, turbulent kinetic energy and temperature. It is very difficult to 'validate' the present parameterisations, either because of a lack of field data, or due to the heterogeneity of urban surfaces that is always very high. Nevertheless, it is possible to find some common features from urban observations that a parameterisation must be able to reproduce. Moreover, an analysis of the differences between the two simulations (*Urban* and *Trad*) is done and the relative impact of the different urban surfaces on the flow is presented. For the analysis a point in the centre of the city and the second day of simulation are chosen.

7.2.1. *Momentum*

A vertical profile of the local u_{*l} (defined as $(\overline{uw(z)}^2 + \overline{vw(z)}^2)^{1/4}$ deduced by fitting a large set of measurements at different hours of the day by Rotach (2001) is presented in Figures 4a, b. The fitting is based on real scale data from different cities, different airflow conditions and with different instruments (Zurich (Rotach, 1993); Basel (Feigenwinter et al., 1999); Sapporo (Oikawa and Meng, 1995)) and from wind-tunnel experiments (Rafailidis, 1997; Kastner-Klein et al., 2001). It shows a maximum at about 2–3 times the average building height and a strong reduction within the canopy; the region below the maximum is usually called the roughness sublayer. Values of the same variable are plotted for the *Urban* and for the *Trad* simulation at two different hours (0000 LST and 1200 LST) for the two test cases. Above the roughness sublayer, the *Urban* (day and night for both geostrophic wind speeds) and the *Trad* simulations (day and night for the strong wind speed and only daytime for the lower wind speed), show a region where u_{*l} is nearly constant with height. This is in agreement with the surface-layer theory (constant flux layer). This layer is shallower for the simulation with lower geostrophic wind speed, since in this case the thermal effects become dominant at a certain height (modification of the wind profile due to the gradient of temperature between the hotter city and the countryside). The strong nocturnal atmospheric stability in the *Trad* simulation with low geostrophic wind reduces the surface-layer height and no region of the constant-flux layer is present. In the roughness sublayer, *Trad* has still a nearly constant-with-height vertical profile of u_{*l} (with a maximum at ground). On the other hand, the vertical profiles computed with the new approach (*Urban*) exhibit a very similar shape as in the observations during night and daytime with a maximum at about 50 m above ground (i.e., the height of the highest building, 2.5 times the average building height) and it corresponds better to the observations.

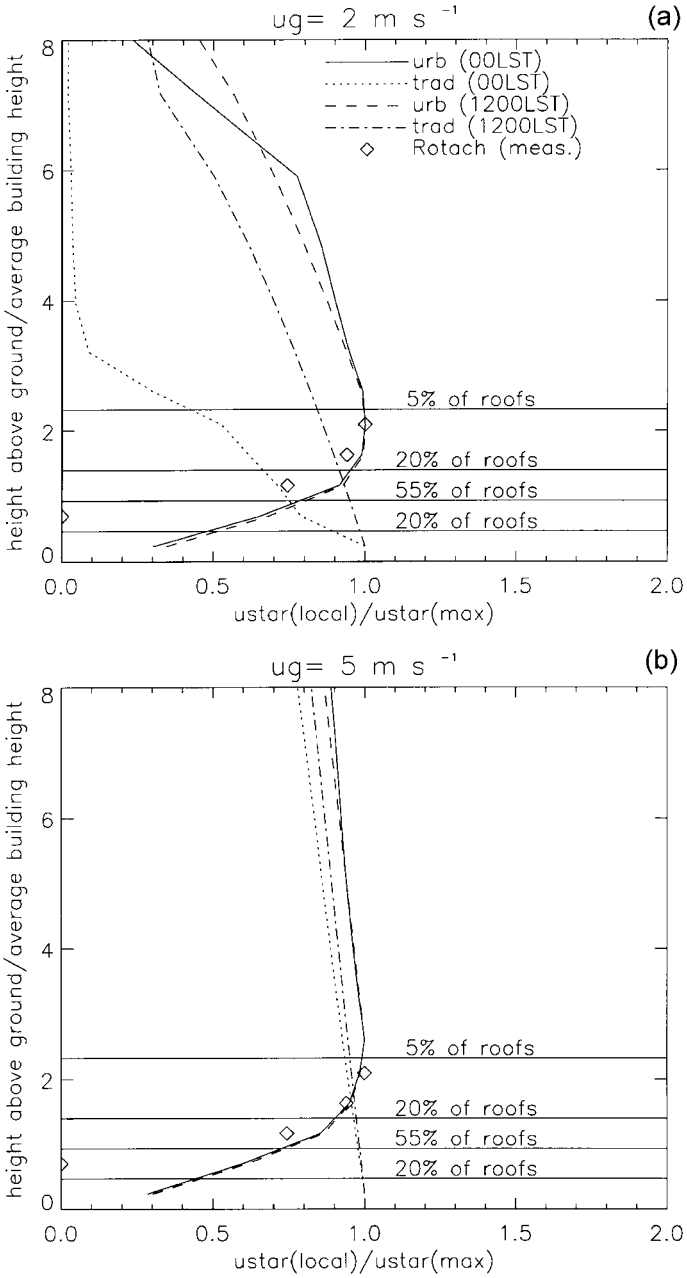

Figure 4. Vertical profiles of the 'local' u_{*l} (defined as $(\overline{uw(z)}^2 + \overline{vw(z)}^2)^{1/4}$), normalised by its maximum value, for the two simulations, during night and daytime for (a) the case with geostrophic wind at 2 m s^{-1}, and (b) 5 m s^{-1}. For comparison, the fitting of different real scale and wind tunnel data (Rotach, 2001) are also plotted. The percentage of roofs refers to the configuration used in the numerical simulation. The results of the *Trad* simulation below the average building height (20 m) are outside their range of applicability.

Another fit of a large set of urban measurements from different sites is presented by Roth (2000) for the ratio between the local u_{*l} and the mean horizontal wind speed. This profile (Figure 5) has a maximum at roof height and then decreases with increasing height reaching a value of 0.1 at around four times the average building height. The vertical profiles computed by the model show a similar behaviour above the average building height, but the *Trad* simulation has a tendency to underestimate this ratio during night-time, with low geostrophic wind, and to overestimate (both during night-time and during daytime) with strong wind. In the new *Urban* simulations, the profiles during night and daytime (both with strong and low geostrophic winds) are quite similar and in better agreement with the curve fitted to the observations. It is important to note that the region below the average building height is not covered by the Roth collection.

These results show that the new *Urban* formulation is able to reproduce the shape of the vertical profiles of the turbulent momentum fluxes in a city better than the traditional approach.

A quantitative comparison between the total momentum sink (sum over horizontal and vertical surfaces) induced by the presence of the buildings in the *Urban* simulation, or

$$M_{\mathrm{tot_{urb}}} = \underbrace{\frac{1}{\Delta x \Delta y} \sum_{iu=1}^{nu} F u_{iu}^{H}}_{\text{horiz.surf}} + \underbrace{\frac{1}{\Delta x \Delta y} \sum_{IU=1}^{nu} F u_{IU}^{V}}_{\text{vert.surf}}$$

on the one hand, and the total momentum sink obtained in the *Traditional* simulation, $M_{\mathrm{tot_{trad}}} = -u_*^2$, is presented in Figure 6. For unstable/neutral conditions (e.g., during daytime) with low geostrophic wind speed (Figure 6), the two simulations give similar values, while during night-time, the values of the *Urban* simulation are much greater than the values of *Trad*. This difference is probably linked with a much stronger atmospheric stability computed in the *Trad* simulation than *Urban* (see details in the next section).

With the new formulation, it is also possible to estimate the relative impact of the horizontal and vertical surfaces on the total sink of momentum. For this configuration (see Table I), the impact of the vertical surfaces is much larger than the impact of roofs and the canyon floor (representing not more than 10% of the total).

One of the most important characteristics of the new formulation is that the momentum sink is not confined to the ground surface, as in *Trad*, but it is vertically distributed up to the highest building. In Figure 7 the percentage of the total momentum sink due to the vertical surfaces (which represent, as explained above, the largest part of the total) at different vertical levels is plotted for 1200 LST and 0000 LST for a point in the centre of the city. The largest part (around 60%) of the momentum sink is located between 10 and 30 m (second and third level). At higher levels, the impact is smaller because of the reduced building density, while

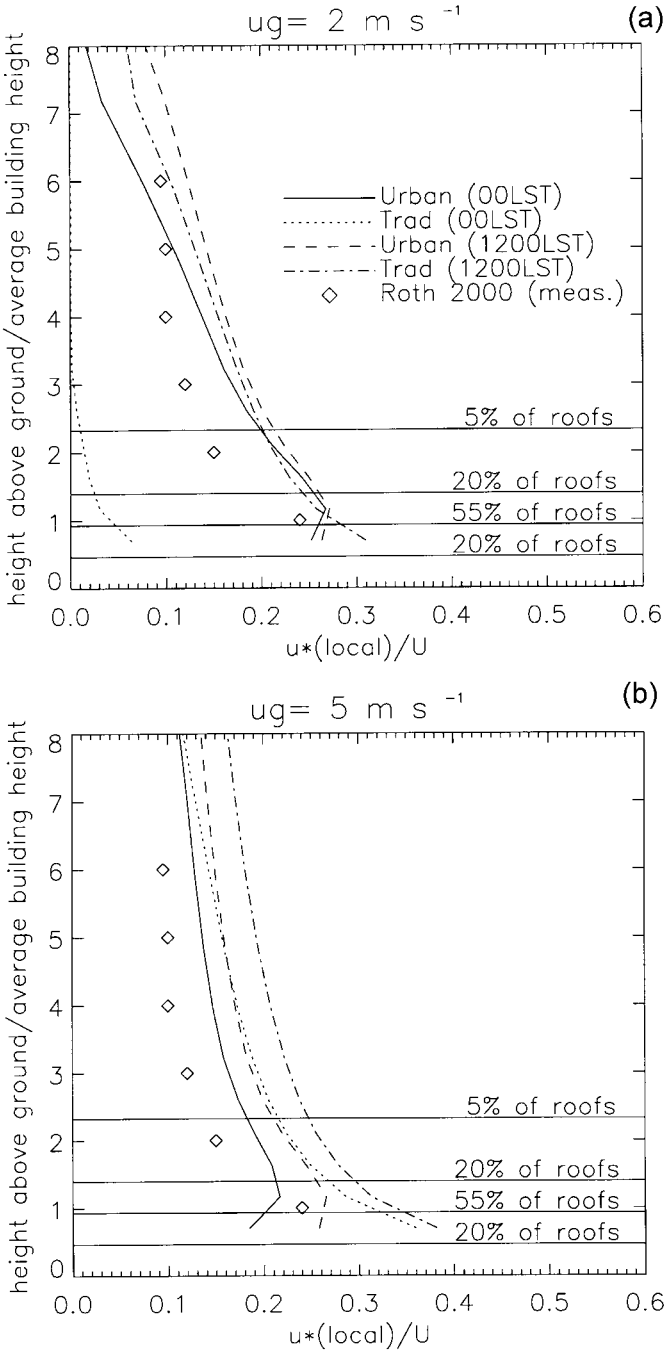

Figure 5. Vertical profiles of the ratio between the local u_{*l}, the mean wind speed and for the two simulations, during night and daytime for (a) the case with geostrophic wind at 2 m s^{-1}, and (b) 5 m s^{-1}. The diamonds refer to an average profile as obtained by Roth (2000) from a large number of full-scale observations. The percentage of roofs refers to the configuration used in the numerical simulation.

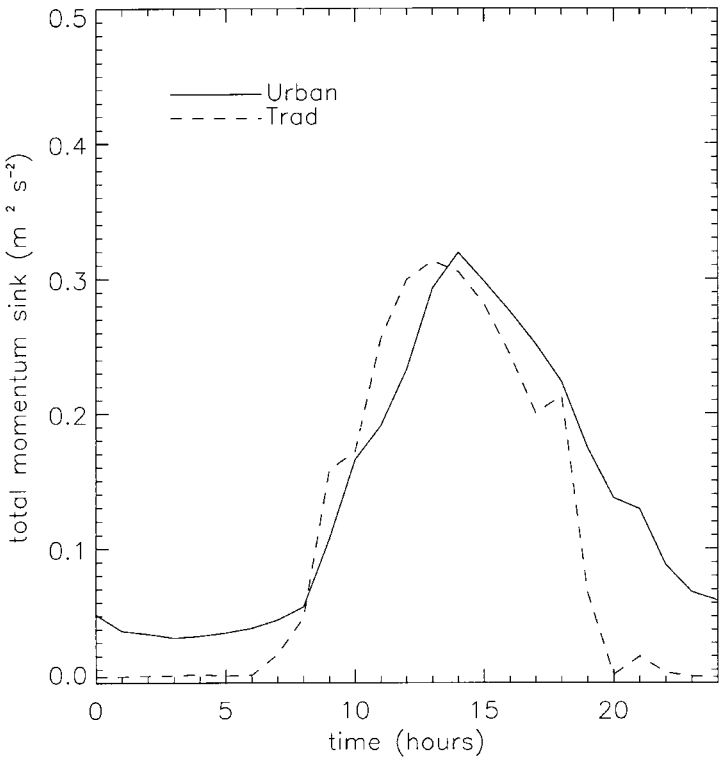

Figure 6. Time variation of the total momentum sink for the two simulations (second day of computations). Results shown for a grid point near the centre of the urban area for the case with geostrophic wind at 2 m s^{-1}.

at the first level the wind is too weak to determine an important drag effect. It is interesting to note that when the thermal effects are dominant (in the case of low wind speed, Figure 7a), the maximum momentum sink during night-time is at a slightly lower altitude as compared to daytime, while with a stronger wind (Figure 7b), when the mechanical effects dominate, the maxima are at the same height. To our knowledge there are not measurements that confirm or deny this trend, but further investigations are needed.

7.2.2. *Temperature*

One of the most important effects induced by a city is the so-called 'Urban Heat Island', which is linked with the fact that the urban canopy is very efficient in trapping radiation and storing heat. Arnfield and Grimmond (1998) derived an empirical formulation (the Objective Hysteresis Model, OHM) to evaluate the total storage of heat for the entire urban canyon as a function of the total radiation of the canyon. Since the OHM has been derived from experimental data, a comparison with this formulation is a good test for the present scheme.

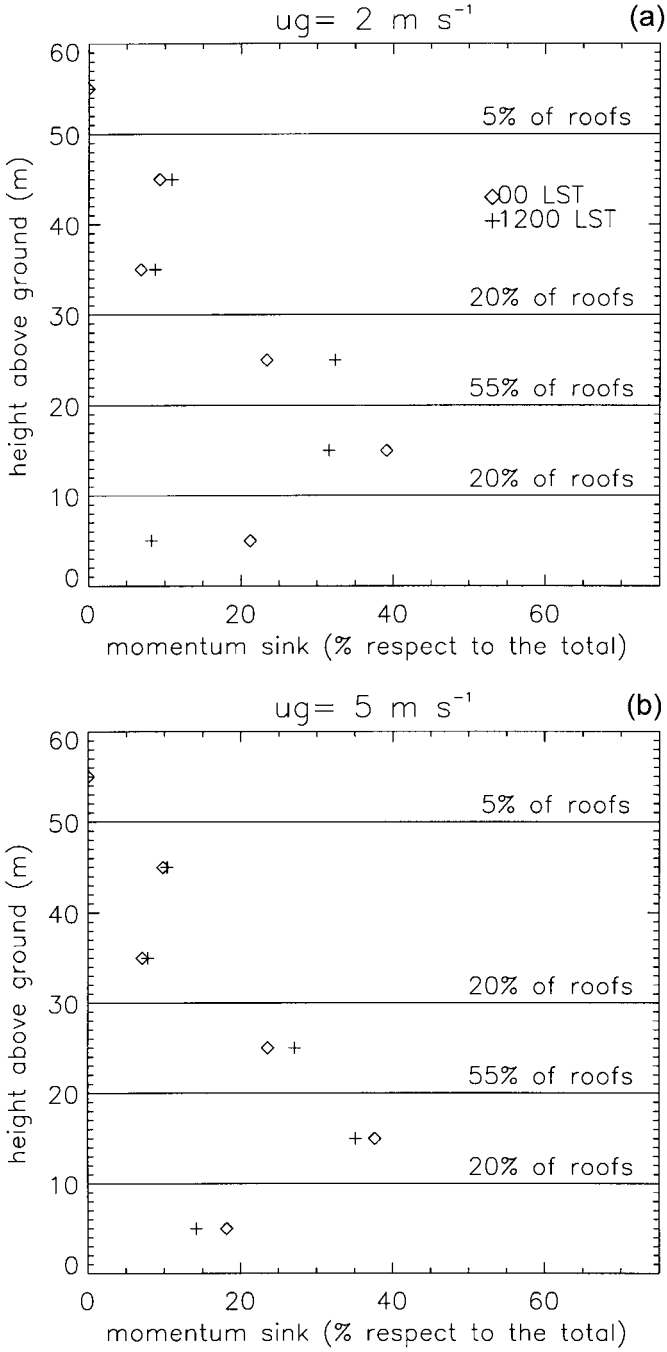

Figure 7. Vertical profile of the contribution to the total sink of momentum due to the wall surfaces during daytime and during nighttime in the *urban* simulation. Results are shown for a grid point near the centre of the urban area for (a) the case with geostrophic wind at 2 m s^{-1}, and (b) 5 m s^{-1}.

In order to have a meaningful comparison, since the OHM refers to a single urban canyon, a one-dimensional (1D) column simulation was run by considering only buildings of 30-m height and a canyon width of 30 m (H/W ratio equal to 1); the street canyon orientation is north-south. Initial wind fields, atmospheric stability, and the other parameters are the same as in the 2D simulation. Again a simulation with the same set-up, but with the *Traditional* approach, was run in parallel.

The total storage of heat ΔQ_{tot} in the urban canyon is defined as (see Appendix A for the meaning of the symbols):

$$\Delta Q_{\text{tot}} = \Delta Q_{\text{floor}} + \frac{1}{W} \sum_{iu=1}^{nu} \Delta z_{iu} (\Delta Q_{iu}^{\text{West}} + \Delta Q_{iu}^{\text{East}}). \tag{25}$$

In Figure 8 model results for the heat storage are compared with the OHM for a three-day simulation. The comparison shows that the new *Urban* formulation is able to reproduce the main characteristics of the phenomena, especially during the night, while the classical *Trad* formulation underestimates the magnitude of the storage (an explanation of the origin of the differences between the two methods is given below, in the global energy budget analysis). The small differences during daytime in model results between the three days are linked with the increase in air temperature from one day to the other. Higher temperatures reduce the differences between the air and surface temperatures and favour the storage. This means that, in general, the amount of energy stored in the urban canyon is not in a fixed ratio with the total radiation, but it can be modified in the case of warm or cold advection.

Considering, again, the 2D simulation (the case with weak synoptic wind) presented at the beginning of the section, it is interesting to analyse the vertical profile of potential temperature during night-time (0000 LST, Figure 9) computed by the model in the centre of the city with the two formulations and at one point (upwind of the city) in the rural area. The profile obtained with the *Urban* set-up shows a neutral layer up to around 150 m above the ground, while the *Trad* profile presents a very stable layer close to the ground, even more stable than that computed by the model in the rural area. The lowest temperatures computed by the *Trad* simulation, as compared to the rural ones, can be explained with a smaller thermal capacity of the concrete (as compared to the moist rural surfaces), and with the enhanced sensible heat fluxes due to the rougher surface. The tendency to a near-neutral layer above a city has been observed very often (e.g., Rotach, 1995) and also the depth of the neutral layer is in agreement with the values (100–300 m) given by Oke (1995).

A detailed analysis of the nocturnal global energy budget (sum over all the surfaces) can explain the differences between the two approaches. In Figure 10, the net radiation, sensible heat flux and storage terms are plotted for the two simulations for night-time hours (second night of the simulations, positive values represent a gain of energy for the surfaces, negative values are a loss of energy). As was shown

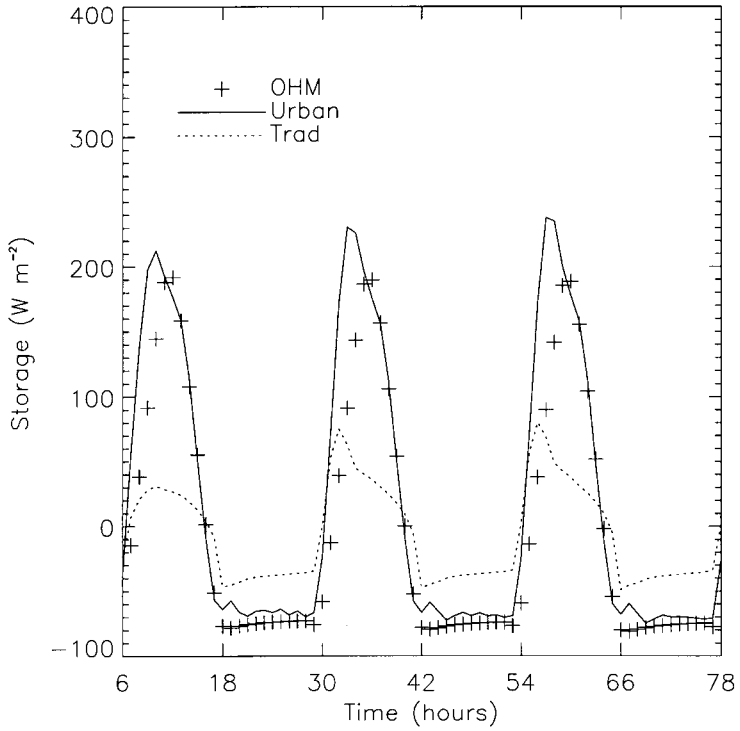

Figure 8. Comparison between simulated values of the heat storage term and the estimation by the OHM (Objective Hysteresis Model, from Arnfield and Grimmond, 1998). Results for the present model refer to a 1D column calculation for a 30-m height and 30-m large street canyon ($H/W = 1$). The parameters chosen for the OHM model are $a1 = 0.43$, $a2 = -0.13$ and $a3 = -44.5$.

in Figure 8, the new formulation *Urban* has a tendency to store more energy in the urban fabric during daytime than *Trad* (in agreement with the results of the OHM model). Consequently, during night-time, more energy is given back to the surface in *Urban* (55–60 W m^{-2}) than in *Trad* (only 25–30 W m^{-2}) (Figure 10a). On the other hand, the global radiation (Figure 10b) is around -50 W m^{-2} in *Urban* and -35 to 40 W m^{-2} in *Trad*; this implies that the restitution of energy to the surface during night-time is able to counterbalance and even overcome the radiation loss only in *Urban* but not in *Trad* (Figure 10c). Responsible for this mechanism is the fact that in *Urban* the radiation loss is attenuated because the radiative trapping in urban canyons is taken into account. These phenomena are very important in the formation of the urban heat island.

It is interesting, now, to understand which role is played by the different urban surfaces in the process. In Figure 11, the sensible heat fluxes from vertical (walls) and horizontal (roof and canyon floor, again positive fluxes means a gain of energy for the surface, while negative are a loss) surfaces are plotted for daytime and night-time. During the day, horizontal surfaces, receiving more direct solar radiation, play a major role. It is also interesting to note that the peaks in sensible heat fluxes from

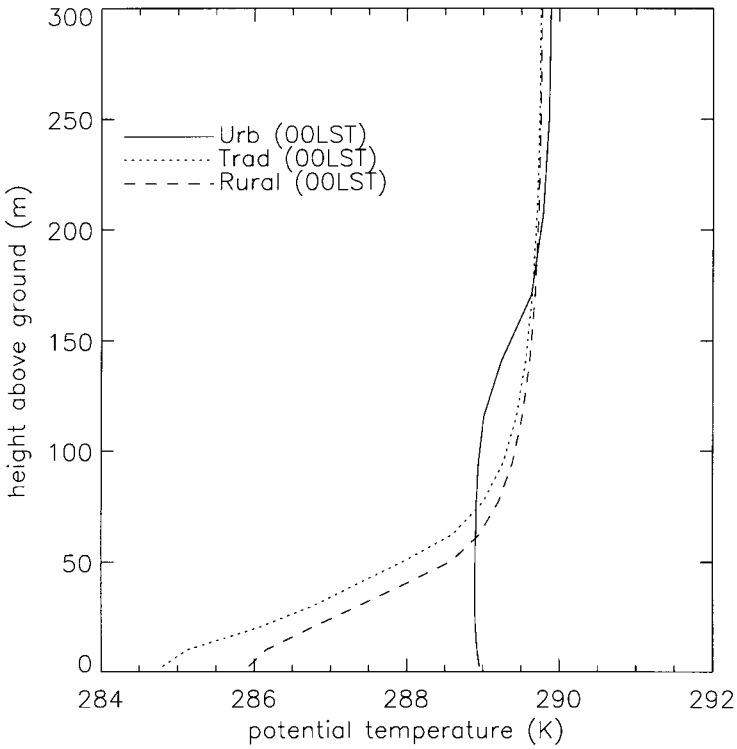

Figure 9. Vertical profiles of potential temperature at midnight as computed by the two simulations at the centre of the urban area and in the rural area, upwind and far from the city for the case with low (2 m s^{-1}) geostrophic wind.

walls are in the morning and in the afternoon, since a north-south oriented street canyon has been chosen for this test simulation. On the other hand, during night the sensible heat flux from horizontal surfaces (which, except the canyon floor, do not experience the radiative trapping) is nearly zero, and all the sensible heat fluxes are from the walls.

7.2.3. *Turbulent Kinetic Energy*

In Figure 12 vertical profiles of the ratio between the turbulent kinetic energy and the square of the maximum local u_{*l} (see definition in the previous section) are plotted for a point in the centre of the city for the two simulations at 0000 LST and 1200 LST; some observations from several urban datasets are also shown. These measurements refer to different urban morphologies and different meteorological situations. Data are quite sparse and diverse, and some show a reduction of TKE in the urban canopy with respect to the value above the canopy, in agreement with a large number of measurements and modelling studies in vegetation canopies (for example, see Raupach et al., 1991), which can be considered similar to an urban

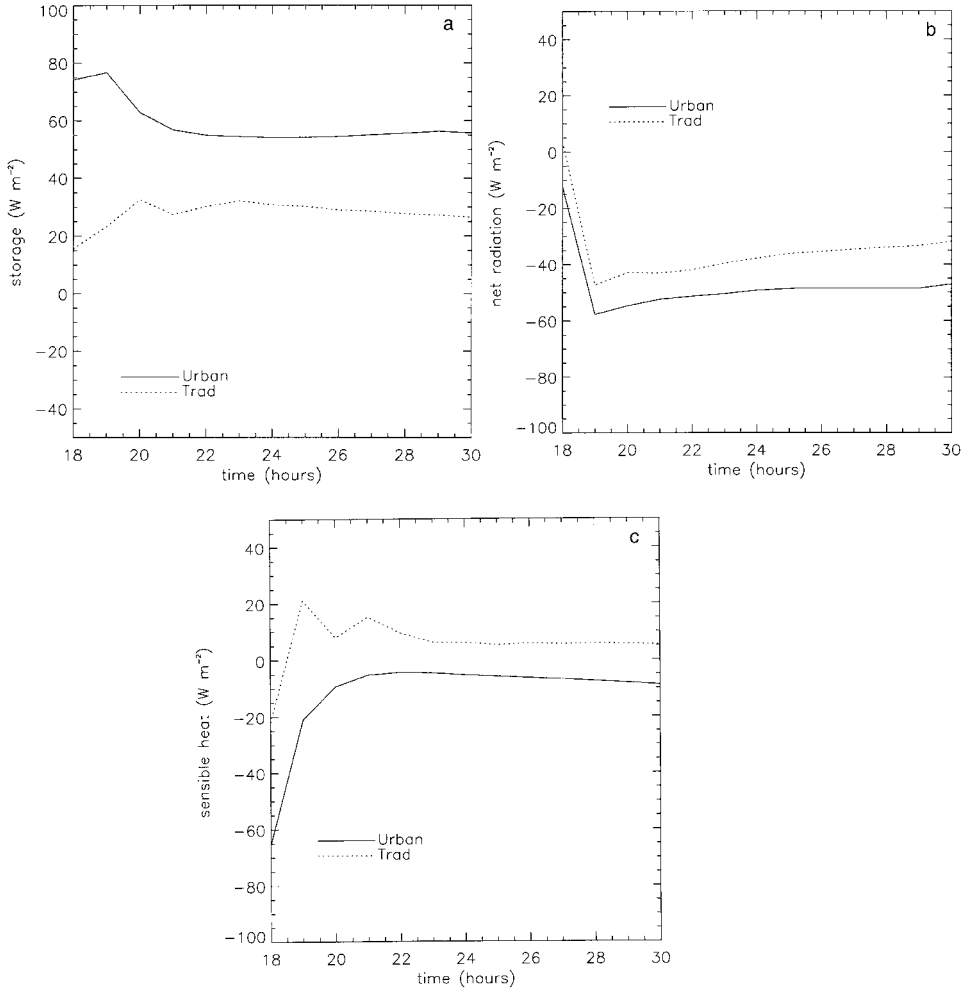

Figure 10. Night-time evolution of the (a) storage terms, (b) net radiation (sum of the direct long and short wave incoming radiation from the sky and the infrared radiation emitted by the surfaces) and (c) sensible heat fluxes and for the two simulations. For the *Urban* simulation a sum over all the surfaces (weighted by the fraction of surface and the density) has been calculated. Positive values represent a gain of energy for the surface and vice versa. Results are for the case with low (2 m s^{-1}) geostrophic wind.

canopy. Moreover, at 2 to 3 times the building height the observed ratio is around 6.

For the simulation with low geostrophic wind speed (Figure 12a), vertical profiles of the *Trad* simulation during night have a maximum at ground and a strong reduction with height. This behaviour is probably linked with the overestimation of the nocturnal atmospheric stability mentioned in the previous paragraph. On the other hand during the day, the profile of the *Trad* simulation shows values larger

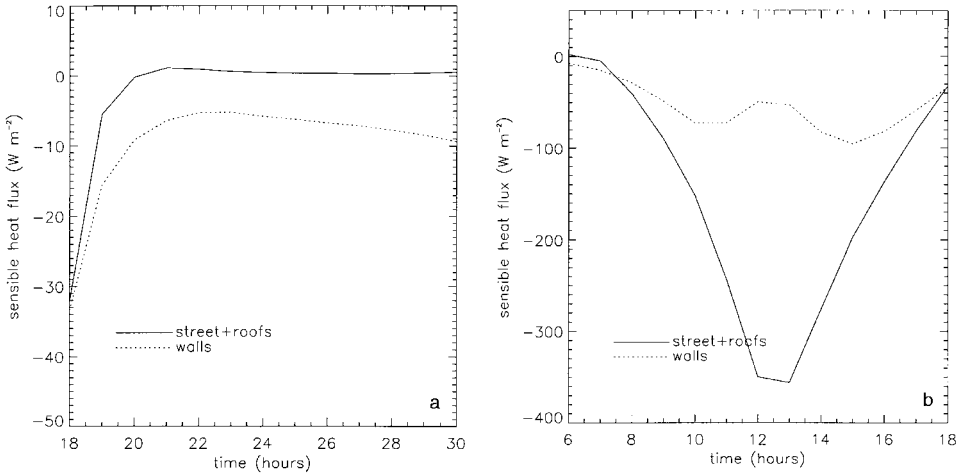

Figure 11. (a) Night-time and (b) daytime evolution of the sensible heat fluxes from horizontal surfaces (roofs and canyon floors) and vertical surfaces (walls). Again, positive values represent a gain of energy for the surface and vice versa. Results are for the case with low (2 m s^{-1}) geostrophic wind.

than 10 already at the second or third vertical numerical level. Results obtained with the new *Urban* formulation have the correct shape and values closer to the observation below 1.5 times the mean building height. Above that height, during the day, *Urban* also overestimates the measured values. In the simulation with stronger geostrophic wind (Figure 12b), where the mechanical effects play a most important role, the values of both simulations are closer to measurements, but *Trad*, as expected, does not reproduce the reduction in TKE in the urban canopy, while *Urban* does. Due to the strong dependence of the TKE on the atmospheric stability, a more complete comparison (and validation) against data for specific real cases is needed.

7.3. Impact on the mesoscale flow

The results presented in the previous section concern mainly the behaviour of the flow close to the urban surface and show that the new model is able to reproduce some of the most important characteristics of the observations recorded in urban areas better than the traditional method. In this section the impact of a city on the global structure of the boundary layer is analysed in order to understand if our simulation results are in agreement with previous observational and numerical studies. The following analysis focuses only on the simulations with weak geostrophic wind, the situation where the thermal effects are more important.

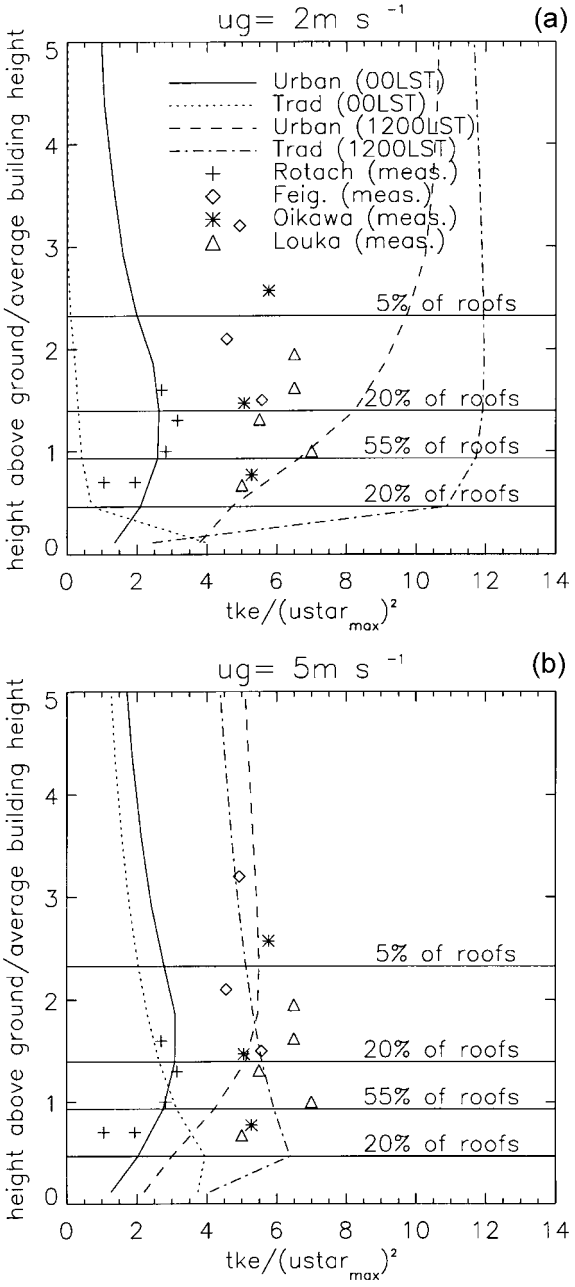

Figure 12. Vertical profiles of turbulent kinetic energy, normalised by the maximum of u_{*l}^2, in a point in the centre of the city for the two simulations during night-time and during daytime of the second day of simulation. For comparison some observations of the same variable from different urban data sets are shown. The percentage of roofs refers to the configuration used in the numerical simulation. Modelling results are (a) from the case with low geostrophic wind speed (2 m s^{-1}) and (b) for the case with strong wind speed (5 m s^{-1}).

7.3.1. *Daytime*

The vertical section of the potential temperature field at 1200 LST (second day), computed in the *Urban* simulation and presented in Figure 13a, clearly shows a vertical plume of warm air developing above the city and displaced downwind by the geostrophic wind. This is due to the fact that sensible heat fluxes in the city area are higher than the corresponding rural fluxes, mainly because in the rural area the energy released to the atmosphere is shared between the latent and the sensible heat fluxes, while in the urban area all the energy is released in the form of sensible heat flux. This effect, together with the stronger turbulent activity generated by the rougher nature of the city, increases the boundary-layer height (represented by the dashed line) from 700 m in the rural area up to 1100 m over the city. The presence of a higher boundary layer above the city as compared to the rural area has been observed, for example, by Spanton and Williams (1988) over London.

The horizontal wind field, presented in Figure 13b, shows very low wind speeds near the city surface and a maximum aloft. This behaviour can be explained by the fact that over the city three forces compete: the drag induced by the urban surface, which is vertically propagated by the turbulent transport of momentum, the pressure gradient resulting from higher temperatures over the city; and the advection induced by the general synoptic flow. These phenomena lead to the low winds near the urban surface, where the drag effects are more important, and a maximum aloft, where the gradient of pressure has the same sign as the advection. The minimum in wind speed downwind of the city arises because the pressure gradient and the synoptic wind advection have opposite signs in this region. The presence of this 'dome' of warm air above the city and the generation of a thermal circulation has been mentioned in several experimental and numerical studies, e.g., Bornstein (1987), Bornstein et al. (1993), Schayes and Grossi (1997). In general, the extension of the influence of the city on the airflow is about 50–60 km in extent (5–6 times the city size) in the horizontal.

The results of the *Trad* simulation are qualitatively similar (not shown), but there are some quantitative differences. In particular, *Trad* simulates a larger boundary-layer height, due to the fact that the sensible heat flux at the ground is higher (since the storage term is lower) than *Urban*, and a greater increase of the wind speed with height close to the surface over the city (since in *Trad* all the momentum sink is at the ground and not vertically distributed up to the highest building).

7.3.2. *Night-time*

During nighttime (2400 LST second night, Figure 13c,d) the situation changes. The temperature field, Figure 13c, shows strong cooling and a very stable atmosphere in the rural area close to the ground. On the other hand, for the reasons already explained, a neutral region of 100–200 m depth is still present above the urban area. In the same region, the horizontal wind is decreased (Figure 13d) by the drag induced by the buildings, vertically propagated by turbulent activity. The increase of wind speed in the city observed in some urban studies (e.g., Bornstein and

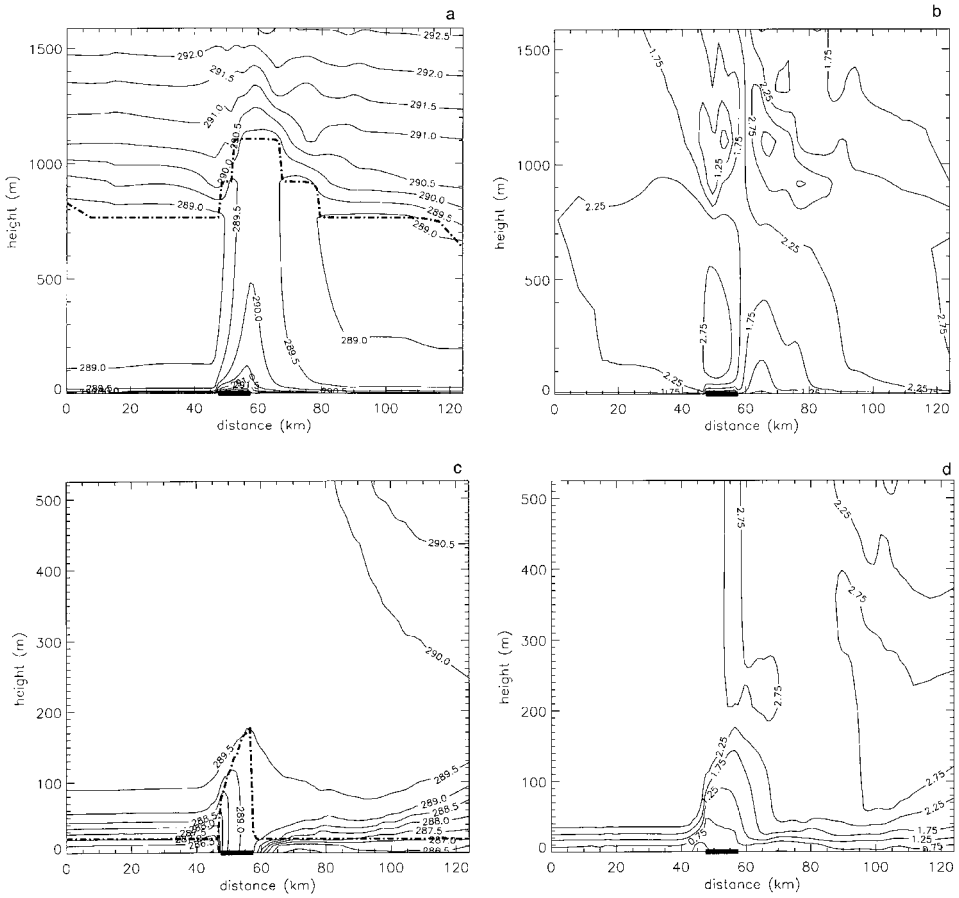

Figure 13. Vertical cross-section of potential temperature ((a) and (c)), horizontal wind ((b) and (d)) for the *Urban* simulation at noon ((a) and (b)) and midnight ((c) and (d)) of the second day. The thick line on the abscissa between 42.5 km and 52.5 km indicates the city location. The dashed line on the potential temperature plots represents the boundary layer height (diagnosed as the level where the turbulent kinetic energy becomes less than 0.01 $m^2 s^{-2}$). Results are for the case with low (2 m s^{-1}) geostrophic wind.

Johnson, 1977; Draxler, 1986) is not reproduced by the model, probably because the urban heat island intensity is not strong enough to overshadow the strong drag induced by the city.

The *Trad* simulation in this case has very different results, since there is a very strong stable layer above the city that prevents the turbulent vertical propagation of the drag induced by the surface. Therefore, the wind decreases only in a very shallow layer (10–20 m depth) above the ground surface (not shown).

Finally, it is important to stress the fact that all these circulations are determined not only by the characteristics of the city itself (structure, dimension, etc.), but also by its interactions with the synoptic forcing and the rural areas. A city surrounded

by a rural area with a very dry soil (e.g., a desert) can experience a very small urban heat island during daytime (in some cases the process can even be reversed). Alternatively, a city with many surfaces of very high albedo can also have a small heat island, and so the strength of the urban heat island is, indeed, strongly dependent on the characteristics of the rural surroundings.

7.4. Impact on the dispersion of a passive tracer

As explained in the Introduction, one of the interests in the study of the urban boundary layer is linked with pollutant dispersion. According to that, it is interesting to study the impact of the city (and of the modifications introduced) on pollutant dispersion.

With this aim the computation of the transport of a passive tracer has been added to the model (same numerical grid, same advection scheme and same turbulent vertical transport as that used in the mesoscale model). The passive tracer is emitted in the city at ground level with a time variation typical of traffic emissions (high values between 0700 LST and 1800 LST and low values during night hours) in order to have realistic profiles. The concentrations computed by the model at the lowest level in the centre of the urban area are plotted in Figure 14. As expected, since the nocturnal boundary layer is much thinner than the diurnal one, the concentrations are higher during the night than during the day. However, since in *Trad* the nocturnal mixing height is only 10–20 m and in *Urban* is 100–150 m, the nocturnal concentrations are much higher in *Trad*. It is important to note here that the problem of an overestimation, with respect to the measurements, of primary pollutants during the night in urban areas is fairly common in Eulerian photochemical models, especially for situations of low winds (for example, Harley et al., 1993; Clappier et al., 2000; Moussioupoulos et al., 1997). These results show that this problem can be linked to an inappropriate reproduction of the nocturnal urban heat island.

Moreover, this fact also has an impact also on daytime pollutant concentration far from the city. In fact, the analysis of the near ground concentrations at 1200 LST (second day, Figure 15) shows that the *Trad* simulation has a 'rural' peak higher and closer to the city than the *Urban* simulation. In the same figure, it is also possible to see also that in the city, the pollutant concentration is higher in *Urban* than in *Trad*. This is in agreement with previous studies (Olesen, 1995; Rotach, 1999, 2001) showing that the traditional parameterisations based on MOST have a tendency to underestimate pollutant concentration during daytime hours (see also Figure 14).

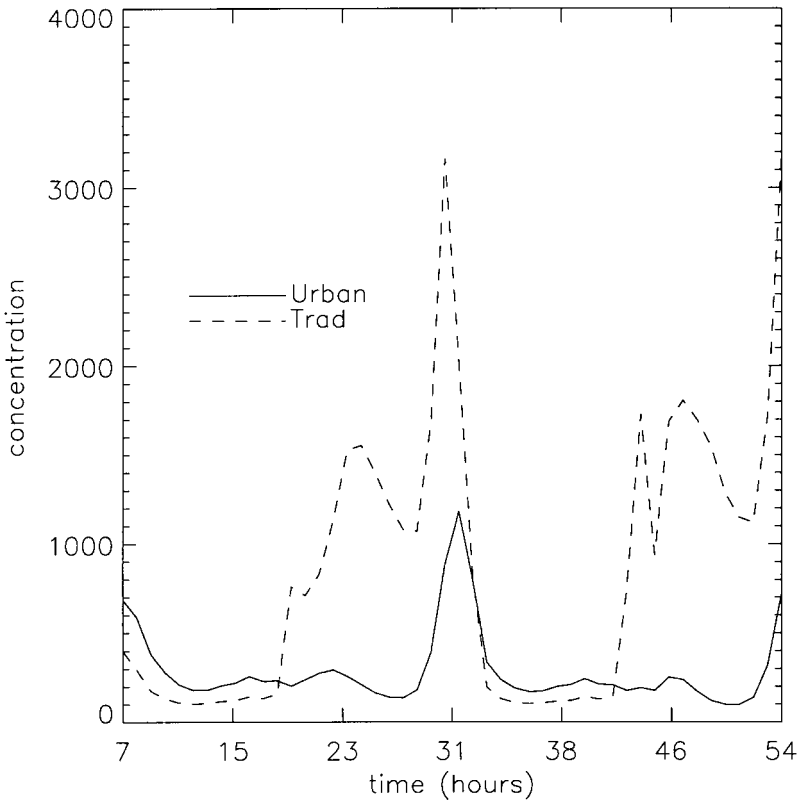

Figure 14. Time evolution of passive tracer surface concentration in the centre of the urban area as computed by the two simulations, *Trad* and *Urban*. Results are for the case with low (2 m s^{-1}) geostrophic wind.

8. Increase in CPU Time

The ratio of computational time between the new routines and the traditional ones depends on the number of levels used in the urban sub-module (this is a function of the vertical resolution of the urban submodule and the maximum building height). For example, in the simulation presented in this work as the test case, the vertical resolution is 10 m, the maximum building height is 50 m (five urban grid levels) and the single routine itself is about two times slower than the traditional one. However, it must be taken into account that the turbulence/diffusion routines usually are responsible for only of 15–20% of the total CPU time of the simulation (the rest is taken by the computation of pressure and advection). Moreover, the region covered by the urban area in a mesoscale domain is hardly larger than 10% of the total (as in the case considered). This explains why the total CPU time of the *Urban* simulation increased by only 3–4% as compared to *Trad*.

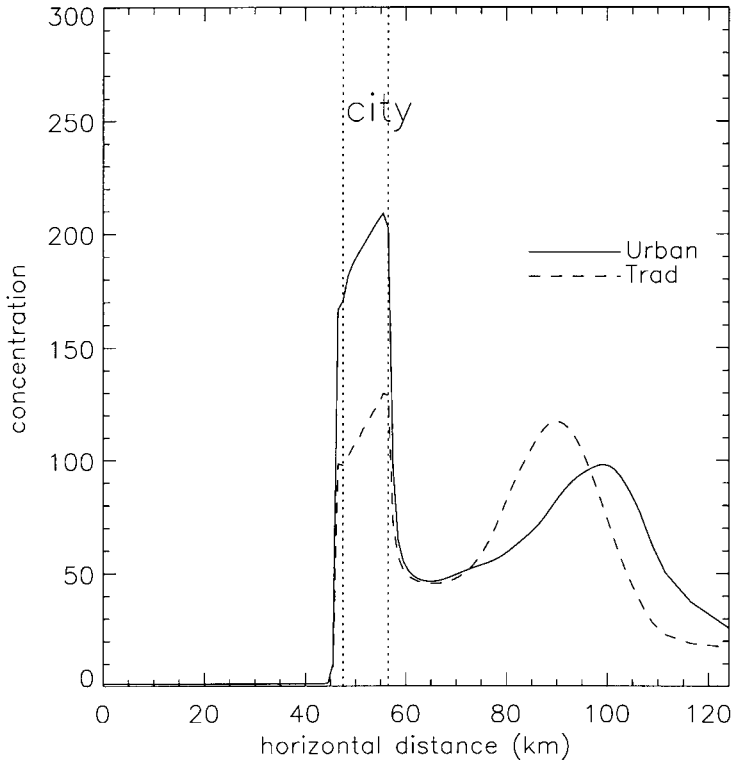

Figure 15. Passive tracer concentration at the lowest level at 1400 LST of the second day. The city is located between 42.5 km and 52.5 km (between the two vertical dotted lines). Results are for the case with low (2 m s^{-1}) geostrophic wind.

9. Conclusions and Perspectives

In this paper, a technique for the computation of turbulent and radiative fluxes in urban areas for mesoscale models has been presented, and where the parameters characterising the city are the building size (in horizontal), the street canyon width and the building density as a function of height. This is different from the traditional approaches, which characterise the city only in terms of high roughness length and a modification to the surface energy budget. The main features of the new technique as compared to the traditional approach are:

1. The sink of momentum is distributed from the ground surface up to the height of the highest building,
2. The shadowing and trapping of radiation in the urban canyon are taken into account.
3. The lengths scales used in the computation of the turbulent kinetic energy are modified by the presence of the buildings.

The new formulation was introduced into a mesoscale model and tested on a simple 2D case characterised by a domain 100 km wide with flat terrain and a

city 10 km large in the centre of the domain. From the comparison between the numerical results obtained with the new formulation and the traditional approach, and with some experimental urban datasets, several conclusions can be drawn:

- *Momentum.* The new parameterisation is able to reproduce qualitatively and quantitatively the increase with height (in magnitude) of the Reynolds stress profiles that is usually observed in measurements, while the traditional approach does not (Figure 4). The total sink of momentum obtained with the new method is comparable to the traditional one during daytime but it is much larger during night-time.
- *Heat.* As compared to the traditional one, the new parameterisation is able to store more energy in the urban fabric during the day, in agreement with the results obtained by the OHM model (Arnfield and Grimmond, 1998). This fact, connected with the reduction in radiation loss during night, permits the formation of a nocturnal urban heat island (this is not possible with the traditional approach). In this mechanism, a very important role is played by the sensible heat fluxes from the vertical surfaces (walls).
- *Turbulence.* The modification of the length scales determines a reduction in the turbulent intensity below the average roof height, as it is usually observed in full scale measurements but which cannot be reproduced with the traditional formulation.

The modifications induced by the presence of a city on the global structure of the boundary layer in model results, for a simple 2D case, show a dome of warm air above the city and the connected thermal circulation above and around the city (with a size of around 4–5 times the city size) during the day, and a neutral layer of 100–200 m depth above the city during the night-time, in agreement with previous experimental and numerical studies.

The differences between the new parameterisation and the traditional approach on passive tracer dispersion emitted in an urban area are mainly lower concentrations during night and higher values during daytime in the urban area with the new parameterisation. Moreover, the position and the intensity of the peak downwind of the city are different.

Possible improvements to the model include:

- to take into account the contribution of parks and urban gardens to the surface energy budget in urban areas;
- to improve the representation of the anthropogenic heat fluxes (partially taken into account in the present formulation by fixing the internal temperature of the walls);
- to make the building morphology spatially variable;
- to take into account the three-dimensionality of the building morphology.

A detailed comparison with turbulent and mean values from full-scale and wind-tunnel experiments could also lead to a refinement of the drag coefficient values and to modifications in the formulation of the turbulent length scales. Overall, it can be

stated that the urban module represents a clear improvement with respect to the traditional approach.

Acknowledgements

The authors would like to thank Dr. Stefano Galmarini for important comments on the first draft of the manuscript. This work was funded by ERCOFTAC.

Appendix A: Computation of the Wall, Street and Roof Temperature

In order to compute the wall, street and roof temperatures, a heat diffusion equation is solved in several layers at the interior of the material (asphalt or concrete):

$$\frac{\partial T_i}{\partial t} = \frac{\partial}{\partial z}\left(K_s \frac{\partial T_i}{\partial z}\right), \tag{A1}$$

where K_s is the substrate thermal conductivity of the material, T_i is the temperature of the ith level in the material. This equation is solved for street, roof and for east and west walls at every model level below the roof level. The internal boundary condition is fixed (this means that the temperature at the deepest level inside the material is constant for the whole simulation period).

At the surface, the boundary condition is defined by solving an energy budget equation (neglecting the latent heat flux), viz.

$$\frac{\partial T_n}{\partial t} = \frac{\left(HF - K_s \left.\frac{\partial T}{\partial z}\right|_{n-1}\right)}{\Delta z g_n}, \tag{A2a}$$

$$HF = \frac{(1-\alpha)Rs + \varepsilon Rl - \varepsilon\sigma T_n^4 + H}{C_s}. \tag{A2b}$$

In this expression α is the albedo of the surface, Rs is the direct and reflected solar radiation received by the surface, ε is the emissivity of the surface, Rl is the long wave radiation received by the surface, H is the sensible heat flux and C_s is the specific heat of the material.

From this, it is possible to define the amount of energy stored in the walls (or roof or canyon floor), i.e., the storage term as:

$$\Delta Q = C_s \left(\Delta z g_n \frac{\partial T}{\partial t} + K_s \left.\frac{\partial T}{\partial z}\right|_{n-1}\right) \tag{A3}$$

This technique is used also in the simulations with the *Traditional* approach in order to compute the surface temperature in urban areas. The difference is that only

one temperature is computed (ground surface) and that the shadow and radiation reflections are not taken into account.

Computation of the Radiation

The method used to compute the radiation in the urban canyon is similar to that of Masson (2000), the main differences being:

1. The lower model level is at the canyon ground and not at the displacement height.
2. There is no integration of the canyon orientations over 360 degrees.
3. Consequently, we keep the distinction between the two facing walls, which have different temperatures, and there can be several numerical levels below the height of the highest building.
4. The equilibrium between the thermodynamic fluxes and the temperature of the air in the canyon is not imposed.
5. The probability of buildings of different heights is taken into account.

These points allow a more detailed computation of the heat fluxes as compared to that of Masson. On the other hand, in his work latent heat flux due to snow melting and anthropogenic heat flux is considered, while in this work, it is neglected.

Longwave radiation (Rl)

As mentioned before the case of a north-south oriented street canyon is analysed, for simplicity, but every orientation is possible. With the assumption that the radiation is reflected at the same rate in all the directions, the longwave radiation reaching the ith element of the western wall Rl_i^W is the sum of the longwave radiation coming from the sky, a fraction of longwave radiation emitted and reflected by the opposite wall and a fraction of the longwave radiation emitted and reflected by the canyon floor,

$$
\begin{aligned}
Rl_{iu}^W = & \underbrace{\Psi_{s,iu}\varepsilon_w Rl_s + \sum_{ju=1,nu} \Psi_{ju,iu}\varepsilon_w Rl_s(1-\Gamma(z_{ju+1}))}_{\text{sky}} \\
& + \underbrace{\varepsilon_g \Psi_{g,iu}\sigma T g^4 + (1-\varepsilon_g)\Psi_{g,iu} Rl_g}_{\text{floor}} \\
& + \underbrace{\sum_{ju=1,nu} \varepsilon_w \Psi_{ju,iu}\sigma T e_{ju}^4 \Gamma(z_{ju+1}) + \sum_{ju=1,nu} (1-\varepsilon_w)\Psi_{ju,iu} Rl_{ju}^E \Gamma(z_{ju+1})}_{\text{wall}},
\end{aligned}
\tag{A4}
$$

where nu is the number of levels in the urban module.

Similarly, for the ith element of the eastern wall we have

$$Rl^E_{iu} = \underbrace{\Psi_{s,iu}\varepsilon_w Rl_s + \sum_{ju=1,nu} \Psi_{ju,iu}\varepsilon_w Rl_s(1-\Gamma(z_{ju+1}))}_{\text{sky}}$$

$$+ \underbrace{\varepsilon_g \Psi_{g,iu}\sigma Tg^4 + (1-\varepsilon_g)\Psi_{g,iu} Rl_g}_{\text{floor}}$$

$$+ \underbrace{\sum_{ju=1,nu} \varepsilon_w \Psi_{ju,iu}\sigma Te^4_{ju}\Gamma(z_{ju+1}) + \sum_{ju=1,nu} (1-\varepsilon_w)\Psi_{ju,iu} Rl^W_{ju}\Gamma(z_{ju+1})}_{\text{wall}}. \tag{A5}$$

Finally, for the street the longwave radiation is

$$Rl_g = \underbrace{\Psi_{s,g} Rl_s + \sum_{ju=1,nu} \Psi_{ju,g} Rl_s(1-\Gamma(z_{ju+1}))}_{\text{sky}}$$

$$+ \underbrace{\sum_{ju=1,nu} \varepsilon_w \Psi_{ju,g}\sigma(Tw^4_{ju} + Te^4_{ju})\Gamma(z_{ju+1}) + \sum_{ju=1,nu} (1-\varepsilon_w)\Psi_{ju,g}(Rl^W_{ju} + Rl^W_{ju})\Gamma(z_{ju+1}),}_{\text{wall}} \tag{A6}$$

where Ψ are the view factors (see below for the details about this calculation). Te, Tw, Tg are surface temperatures of eastern and western walls and canyon floor, respectively. If the surface temperatures of the previous time step are used, this is a linear system of $2n+1$ equations and $2n+1$ unknowns (the longwave radiation at walls and street, with n the number of levels below the roof height), which is easy to solve by a matrix inversion.

SHORTWAVE (OR SOLAR) RADIATION (Rs)

The solar radiation captured by a wall is the sum of the direct radiation coming from the sky and the radiation reflected by the other components of the canyon. Assuming that the surfaces of the walls and the ground are rough enough to reflects the shortwave radiation isotropically in all the directions, we have for the ith element of the western wall

$$Rs^W_{iu} = \underbrace{Rs^W_{s,iu} + \sum_{ju=1,nu} \Psi_{ju,iu} Rs^W_{s,ju}(1 - \Gamma(z_{ju+1}))}_{\text{sky}} + \underbrace{\alpha_g \Psi_{g,iu} Rs_g}_{\text{floor}}$$

$$+ \underbrace{\sum_{ju=1,nu} \alpha_w \Psi_{ju,iu} Rs^E_{ju} \Gamma(z_{ju+1})}_{\text{wall}}, \tag{A7}$$

for the ith element of the eastern wall,

$$Rs^E_{iu} = \underbrace{Rs^E_{s,iu} + \sum_{ju=1,nu} \Psi_{ju,iu} Rs^E_{s,ju}(1 - \Gamma(z_{ju+1}))}_{\text{sky}} + \underbrace{\alpha_g \Psi_{g,iu} Rs_g}_{\text{floor}}$$

$$+ \underbrace{\sum_{ju=1,nu} \alpha_w \Psi_{ju,iu} Rs^W_{ju} \Gamma(z_{ju+1})}_{\text{wall}}, \tag{A8}$$

and for the ground,

$$Rs_g = \underbrace{Rs_{s,g} + \sum_{ju=1,nu} \Psi_{ju,g}(Rs^W_{s,ju} + Rs^E_{s,ju})(1 - \Gamma(z_{ju+1}))}_{\text{sky}}$$

$$+ \underbrace{\sum_{ju=1,nu} \alpha_w \Psi_{ju,g}(Rs^W_{ju} + Rs^E_{ju})\Gamma(z_{ju+1})}_{\text{wall}}. \tag{A9}$$

This is, again, a linear system of $2n+1$ equations in $2n+1$ unknowns (the shortwave radiation at walls and ground).

To compute the direct radiation we have to take into account the obstruction of the canyon elements. Let us first consider the case of a canyon perpendicular to the sun direction. For a horizontal surface, the energy arriving at the ith element of the vertical wall will be equal to Rs (the value of direct solar radiation at ground on a horizontal unit cross-sectional area) multiplied by the projection on the horizontal plane of the portion of the element receiving light divided by the area of the element. Referring to Figure A1, this yields

$$Rs_{s,iu} = \frac{Rs}{z_{iu+1} - z_{iu}} \sum_{ju=1}^{nu} [\max(0., x1 - x2)\gamma(z_{ju+1})], \tag{A10}$$

with $x1 = \min((z_{ju+1} - z_i) \tan Zr, W)$, and $x2 = \max(0., (z_{ju+1} - z_{i+1}) \tan Zr)$, and with Zr the solar zenith angle.

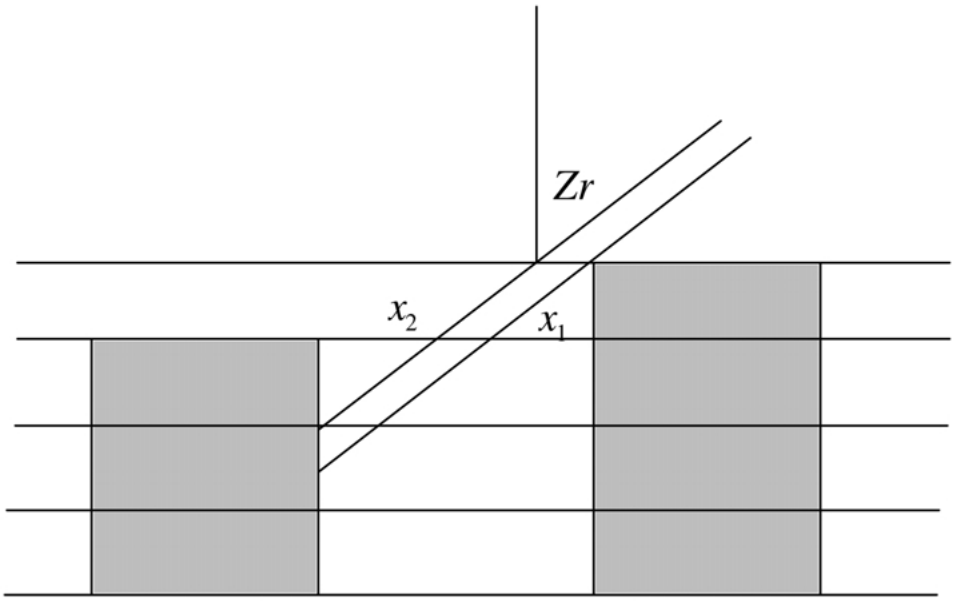

Figure A1. Computation of the shadowing effects; Zr is the solar zenith angle.

For the canyon floor we obtain:

$$Rs_{s,g} = \frac{Rs}{W} \sum_{ju=1}^{nu} [\max(0., W - z_{ju+1} \tan Zr)\gamma(z_{ju+1})]. \tag{A11}$$

In order to take into account other canyon orientations, one should replace W in Equations (A10) and (A11) by $W/\sin\chi$ and multiply the wall fluxes by $\sin\chi$ (Equations (A7) to (A9)).

The formula used to compute the angle χ between the sun direction and the face of the wall is from Pielke (1984),

$$\chi = \arcsin\left(\frac{\cos(\delta_{\text{sum}})\sin(h_r)}{\sin(Zr)}\right) - D_{\text{street}}, \tag{A12}$$

with δ_{sun} the solar declination, h_r the hour angle and D_{street} the street direction.

Computation of the view factors

A detailed explanation of the technique used in the computation of the view factors can be found in Sparrow and Cess (1978). Only the formulae used in this work are reported here. Let us first define two functions f_{prl} and f_{nrm}, which are the angle factors between two equal and parallel planes, f_{prl}, and two equal and orthogonal planes, f_{nrm}, respectively:

$$f_{prl}(a,b,c) = \left(\frac{2}{\pi XY}\right)\left(\ln\left[\frac{(1+X^2)(1+Y^2)}{1+X^2+Y^2}\right]^{1/2}\right.$$
$$+Y\sqrt{1+X^2}\tan^{-1}\left(\frac{Y}{\sqrt{1+X^2}}\right)$$
$$\left.+\,X\sqrt{1+Y^2}\tan^{-1}\left(\frac{X}{\sqrt{1+Y^2}}\right)-Y\tan^{-1}Y-X\tan^{-1}X\right) \tag{A13}$$

where $X = a/c$, $Y = b/c$, and a and b are the two dimensions of the surfaces, and c is the distance between the surfaces,

$$f_{nrm}(a,b,c) = \left(\frac{1}{\pi Y}\right)\left(\frac{1}{4}\left(\ln\left(\frac{(1+X^2)(1+Y^2)}{1+Z}\right)+Y^2\ln\left(\frac{Y^2(1+Z)}{Z(1+Y^2)}\right)\right.\right.$$
$$+X^2\ln\left(\frac{X^2(1+Z)}{Z(1+X^2)}\right)\Bigg)+Y\tan^{-1}\left(\frac{1}{Y}\right)+X\tan^{-1}\left(\frac{1}{X}\right)$$
$$\left.-\sqrt{Z}\tan^{-1}\left(\frac{1}{\sqrt{Z}}\right)\right), \tag{A14}$$

with, this time, $X = a/b$, $Y = c/b$, $Z = X^2 + Y^2$, and b is the dimension of the side common for the two surfaces, while a and c are the other two dimensions of the surfaces.

At this point using the angle-factor algebra it is possible to compute the view factors for every element. In particular for wall-to-wall terms, like Ψ_{ij}, the view factor for the radiation emitted by the wall element j and received by the element i is:

$$\Psi_{ji} = \frac{1}{2}((|z_{i+1}-z_j|)f_{prl}(D,|z_{i+1}-z_j|,W)$$
$$-|z_{i+1}-z_{j+1}|f_{prl}(D,|z_{i+1}-z_{j+1}|,W)$$
$$-|z_i-z_j|f_{prl}(D,|z_i-z_j|,W)$$
$$+|z_i-z_{j+1}|f_{prl}(D,|z_i-z_{j+1}|,W))\frac{1}{|z_{i+1}-z_i|} \tag{A15}$$

with D the length of the street canyon (equal to the grid dimension), W width of the street, z_i the height above ground of the face of the ith levels. The division by the surface of the receiving element is done in order to have a flux of energy (W m^{-2}).

For canyon-ground-to-wall terms we have:

$$\Psi_{gi} = (f_{nrm}(z_{i+1},D,W) - f_{nrm}(z_i,D,W))\frac{W}{z_{i+1}-z_i}. \tag{A16}$$

For walls-to-canyon-ground terms similarly:

$$\Psi_{ig} = (f_{nrm}(W, D, z_{i+1})z_{i+1} - f_{nrm}(W, D, z_i)z_i)\frac{1}{W}. \tag{A17}$$

For sky-to-wall

$$\Psi_{si} = (f_{nrm}(H - z_i, D, W) - f_{nrm}(H - z_{i+1}, D, W))\frac{W}{z_{i+1} - z_i}, \tag{A18}$$

with H the maximum building height.

For sky-to-ground terms, finally, we have

$$\Psi_{sg} = f_{prl}(D, W, H). \tag{A19}$$

Appendix B: Connection with the Mesoscale Model

Since the numerical grid where the urban fluxes are computed can be different from the grid of the mesoscale model, a procedure of averaging/interpolation is needed to connect the two grids.

B.1. Mesoscale to urban

The computation of the fluxes induced by the presence of the buildings requires the values of the wind and air temperature as input. A volumetric interpolation of these values from the 'mesoscale' grid (the grid where these values are computed) to the urban grid is performed. For a variable A (wind or temperature), referring to Figure 2, this interpolation is performed according to:

$$A_{IU} = \frac{1}{z_{iu+1} - z_{iu}} \sum_{i=ib-1}^{ie} (\min(Z_{i+1}, z_{iu+1}) - \max(Z_i, z_{iu}))A_I \tag{B1}$$

with ib and ie the lowest and the highest mesoscale model levels within the IU urban levels.

B.2. Urban to mesoscale

The new term D_A (for a variable a that can be wind speed, temperature or TKE, see description Section 2) for urban areas is given by Equation (20). Referring to Figure 2, the terms used in Equation (20) are computed in the following way. For horizontal surfaces,

$$Fa_I^H = \sum_{iu=iub}^{iue} Fa_{iu}^H, \tag{B2}$$

where iub and iue are, respectively, the lowest and the highest urban grid level in the grid of the mesoscale model. For the vertical surfaces:

$$Fa_I^V = \frac{1}{Z_{i+1} - Z_i} \sum_{iu=iub-1}^{iue} (\min(Z_{i+1}, z_{iu+1}) - \max(Z_i, z_{iu})) Fa_{IU}^V. \tag{B3}$$

The surface between grid cell I and grid cell $I-1$ not occupied by buildings, S_i^A, used in Equation (21) is:

$$S_i^A = S_{\text{tot}}^H \frac{W + (1 - \gamma(Z_i))B}{W + B}. \tag{B4}$$

The air volume of the cell is also modified due to the presence of the buildings,

$$V_I^A = V_{\text{tot}I} \left(1 - \frac{B}{W + B} \sum_{i=ib}^{ie} \Gamma(z_{iu+1})(\min(Z_{i+1}, z_{iu}) - \max(Z_i, z_{iu})) \right), \tag{B5}$$

with $V_{\text{tot}I}$ being the total volume of the cell (building + air).

This technique is valid for the terms in the momentum and temperature equations and for the fluxes from vertical surfaces in the turbulent kinetic energy equation.

A different manipulation is needed for the shear and buoyancy terms (Pr) in the TKE equation, since they are volumetric. The approach adopted is the following

$$\text{Pr}_I = \sum_{iu=iub}^{iue} S_{iu}^H \Delta z_{IU} (\text{Pr}_{IU}^H) + \left(V_I - \sum_{iu=iub}^{iue} S_{iu}^H \Delta z_{IU} \right) \text{Pr}_{IU}^{\text{trad}}, \tag{B6}$$

where $\text{Pr}_{IU}^{\text{trad}}$ are the shear and buoyant production terms computed in the traditional way (see Section 2).

References

Arnfield, A. J. and Grimmond, C. S. B.: 1998, 'An Urban Canyon Energy Budget Model and its Application to Urban Storage Heat Flux Modelling', *Energ. Buildings* **27**, 61–68.

Ashie, Y., Vu Thanh Ca, and Asaeda, T.: 1999, 'Building Canopy Model for the Analysis of Urban Climate', *J. Wind Eng. Ind. Aero.* **81**, 237–248.

Ayotte, K. W., Finnigan, J. J., and Raupach, M. R.: 1999, 'A Second-Order Closure for Neutrally Stratified Vegetative Canopy Flows', *Boundary-Layer Meteorol.* **90**, 189–216.

Bornstein, R. D.: 1987, 'Mean Diurnal Circulation and Thermodynamic Evolution of Urban Boundary Layers', in *Modelling the Urban Boundary Layer*, American Meteorological Society, Boston, MA, pp. 53–94.

Bornstein, R. D. and Johnson, D. S.: 1977, 'Urban-Rural Wind Velocity Differences', *Atmos. Environ.* **11**, 597–604.

Bornstein, R. D., Thunis, P., and Schayes, G.: 1993, 'Air Pollution in Coastal Urban Flows: Observations and Model Evaluation for the New York City Area', in *Proceedings of the Apsis Meeting*, April, Lausanne, Switzerland, pp. 29–30.

Bottema, M.: 1997, 'Urban Roughness Modelling in Relation to Pollutant Dispersion', *Atmos. Environ.* **31**, 3059–3075.

Bougeault, P. and Lacarrere, P.: 1989, 'Parameterisation of Orography-Induced Turbulence in a Mesobeta-Scale Model', *Mon. Wea. Rev.* **117**, 1872–1890.

Brown, M: 2000, 'Urban Parameterisations for Mesoscale Meteorological Models', in Z. Boybey (ed.), *Mesoscale Atmospheric Dispersion*, Wessex Press, 448 pp.

Brown, M. and Williams, M: 1998, 'An Urban Canopy Parameterisation for Mesoscale Meteorological Models', in *AMS 2nd Urban Environment Symposium*, Albuquerque, NM.

Clappier, A.: 1998, 'A Correction Method for Use in Multidimensional Time-Splitting Advection Algorithms: Application to Two and Three Dimensional Transport', *Mon. Wea. Rev.* **126**, 232–242.

Clappier, A., Martilli, A., Grossi P., Thunis, P., Pasi, F., Krueger, B. C., Calpini, B., Graziani, G., and van den Bergh, H.: 2000, 'Effect of Sea Breeze on Air Pollution in the Greater Athens Area. Part 1: Numerical Simulations and Field Observations', *J. Appl. Meteorol.* **39**, 546–562.

Clappier, A., Martin, M., Chopard, B., and van den Bergh, H.: 1997, 'Unified Modelling of Meteorology and Air Pollution on Massively Parallel Computers', Swiss National Fund final report no. 21045625.25.

Clappier, A., Perrochet. P., Martilli, A., Muller, F., and Krueger, B. C.: 1996, 'A New Non-hydrostatic Mesoscale Model using a CVFE (Control Volume Finite Element) Discretisation Technique', in P. M. Borrell et al. (eds.), *Proceedings of EUROTRAC Symposium '96*, Computational Mechanics Publications, Southampton, pp. 527–531.

Clarke, J. A.: 1985, *Energy Simulation in Building Design*, Adam Hilger, Bristol, 362 pp.

Collella, P. and Woodward, P.: 1984, 'The Piecewise Parabolic Method (PPM) for Gas Dynamical Simulations', *J. Comp. Phys.* **54**, 174–201.

Draxler, R. R.: 1986, 'Simulated and Observed Influence of the Nocturnal Urban Heat Island on the Local Wind Field', *J. Appl. Meteorol.* **25**, 1125–1133.

Duynkerke, P. G.: 1988, 'Application of the E-Epsilon Turbulence Closure Model to the Neutral and Stable Atmospheric Boundary Layer', *J. Atmos. Sci.* **45**, 865–880.

Feigenwinter, C., Vogt, R., and Parlow, E.: 1999, 'Vertical Structure of Selected Turbulence Characteristics above an Urban Canopy', *Theor. Appl. Climatol.* **62**, 51–63.

Grimmond, C. S. B. and Oke, T. R.: 2000, 'Aerodynamic Properties of Urban Areas Derived from Analysis of Surface Form', *J. Appl. Meteorol.* **38**, 1262–1292.

Harley, R. A., Russell, A. G., McRae, J., Cass, G. K., and Seinfeld, J. H.: 1993, 'Photochemical Air Quality Modelling of the Southern California Air Quality Study', *Environ. Sci. Technol.* **27**, 378–388.

Kastner-Klein, P., Fedorovich, E., and Rotach, M.: 2001, 'A Wind Tunnel Study of Organised and Turbulent Air Motions in Urban Street Canyons', *J. Wind Eng. Ind. Aerodyn.* **89**, 849–861.

Louis, J. F.: 1979, 'A Parametric Model of Vertical Eddies Fluxes in the Atmosphere', *Boundary-Layer Meteorol.* **17**, 187–202.

Louka, P., Belcher, S. E., and Harrison, R. G.: 2000, 'Coupling between Air Flow in Streets and the Well Developed Boundary Layer Aloft', *Atmos. Environ.* **34**, 2613, 2621.

Martilli, A.: 2001, *Development of an Urban Turbulence Paramterisation for Mesoscale Atmospheric Models*, Ph.D. Dissertation, Swiss Federal Institute of Technology, Lausanne, Switzerland, 192 pp.

Masson, V.: 2000, 'A Physically-Based Scheme for the Urban Energy Budget in Atmospheric Models', *Boundary-Layer Meteorol.* **94**, 357–397.

Moussioupouolos, N., Sahm, P., Karatzas, K., Papalexiou, S., and Karagianidis, A.: 1997, 'Assessing the Impact of the New Athens Airport to Urban Air Quality with Contemporary Air Pollution Models', *Atmos. Environ.* **31**, 1497–1511.

Oikawa, S. and Meng, Y.: 1995, 'Turbulence Characteristics and Organised Motions in a Suburban Roughness Sublayer', *Boundary-Layer Meteorol.* **74**, 289–312.

Oke, T. R.: 1995, 'The Heat Island of the Urban Boundary Layer: Characteristics, Causes and Effects', in J. E. Cermak et al. (eds.), *Wind Climate in Cities*, Kluwer Academic Publishers, Dordrecht, Boston, pp. 81–107.

Olesen, H. R.: 1995, 'The Model Validation Exercise at Mol: Overview of Results', *Int. J. Environ. Poll.* **5**, 761–784.

Pielke, R.: 1984, *Mesoscale Meteorological Modelling*, Academic Press, San Diego, 612 pp.

Rafailidis, S.: 1997, 'Influence on Building Areal Density and Roof Shape on the Wind Characteristics above a Town', *Boundary-Layer Meteorol.* **85**, 255–271.

Raupach, M. R.,: 1992, 'Drag and Drag Partition on Rough Surfaces', *Boundary-Layer Meteorol.* **60**, 375–395.

Raupach, M. R. and Shaw, R. H.: 1982, 'Averaging Procedure for Flow within Vegetation Canopies', *Boundary-Layer Meteorol.* **22**, 79–90.

Raupach, M. R., Antonia, R. A., and Rajagoplan, S.: 1991, 'Rough-Wall Turbulent Boundary Layers', *Appl. Mech. Rev.* **44**, 1–25.

Rhie, C. M. and Chow, W. L.: 1983, 'Numerical Study of the Turbulent Flow as an Airfoil with Trailing Edge Separation', *AIAA J.* **21**, 1525–1532.

Rotach, M. W.: 1993, 'Turbulence Close to a Rough Urban Surface. Part 1: Reynolds Stress', *Boundary-Layer Meteorol.* **65**, 1–28.

Rotach, M. W.: 1995, 'Profiles of Turbulence Statistics in and above an Urban Street Canyon', *Atmos. Environ.* **29**, 1473–1486.

Rotach, M. W.: 1999, 'On the Influence of the Urban Roughness Sublayer on Turbulence and Dispersion', *Atmos. Environ.* **33**, 4001–4008.

Rotach, M. W.: 2001, 'Urban Scale Dispersion Modelling Using a Lagrangian Particle Dispersion Model', *Boundary-Layer Meteorol.* **99**, 379–410.

Roth, M.: 2000, 'Review of Atmospheric Turbulence over Cities', *Quart. J. Roy. Meteorol. Soc.* **126**, 1941–1990.

Sasamori, T.: 1968, 'Radiative Cooling Calculation for Application to General Circulation Experiments', *J. Appl. Meteorol.* **7**, 721–729

Schayes, G.: 1982, 'Direct Determination of Diffusivity Profiles form Synoptic Reports', *Atmos. Environ.* **16**, 1407–1413.

Schayes, G. and Grossi, P.: 1997, 'Sensitivity Analysis on Boundary Layer Height on Idealised Cities', in *Proceedings of EURASAP Workshop on the Determination of the Mixing Height*, Risoe National Laboratory, Roskilde, Denmark, 1–3 October.

Sievers, U.: 1990, 'Dreidimensionale Simulation in Stadtgebieten. Schriftenreihe Umweltmeteorologie Band 15', in *Kommission Reinhaltung der Luft im VDI und DIN*, Dusseldorf, pp. 36–43 (in German).

Spanton, A. M. and Williams, M. L.: 1988, 'A Comparison of the Structure of the Atmospheric Boundary Layers in Central London and a Rural/Suburban Site Using Acoustic Sounding', *Atmos. Environ.* **22**, 211–223.

Sparrow, E. M. and Cess, R. D.: 1978, *Radiation Heat Transfer*, Brooks/Cole Publishing Company, Belmnot, CA, 366 pp.

Tremback, C. J. and Kessler, R.: 1985, 'A Surface Temperature and Moisture Parameterisation for use in Mesoscale Numerical Models', in *Proceedings of 7th Conference on Numerical Weather Prediction*, June 17–20, Montreal, Quebec, Canada.

Uno, I., Ueda, H., and Wakamatsu, S.: 1989, 'Numerical Modelling of the Nocturnal Urban Boundary Layer', *Boundary-Layer Meteorol.*, **49**, 77–98.

Wilson, N. and Shaw, R.: 1977, 'A Higher Order Closure Model for Canopy Flow', *J Appl. Meteorol.* **16**, 1197–1205.

Yamada, T.: 1982, 'A Numerical Study of Turbulent Airflow in and above a Forest Canopy', *J. Meteorol. Soc. Japan* **60**, 439–454